

PAPER

## Ordered hexagonal patterns via notch–delta signaling

To cite this article: Eyal Teomy *et al* 2021 *Phys. Biol.* **18** 066006

View the [article online](#) for updates and enhancements.

### You may also like

- [An integrative model of cancer cell differentiation with immunotherapy](#)  
David H Margarit, Nadia S González, Lilia M Romanelli *et al.*

- [Cellular Tango: how extracellular matrix adhesion choreographs Rac-Rho signaling and cell movement](#)  
Elisabeth G Rens and Leah Edelstein-Keshet

- [SARS-coronavirus-2 infections: biological instabilities characterized by order parameters](#)  
T D Frank



**IOP | ebooks™**

Bringing together innovative digital publishing with leading authors from the global scientific community.

Start exploring the collection—download the first chapter of every title for free.

# Physical Biology



## PAPER

# Ordered hexagonal patterns via notch–delta signaling

RECEIVED  
11 February 2021

REVISED  
18 August 2021

ACCEPTED FOR PUBLICATION  
21 September 2021

PUBLISHED  
21 October 2021

Eial Teomy<sup>1,4</sup>, David A Kessler<sup>1,\*</sup>  and Herbert Levine<sup>2,3</sup> 

<sup>1</sup> Department of Physics, Bar-Ilan University, Ramat-Gan 52900, Israel

<sup>2</sup> Dept of Physics, Northeastern Univ., Boston MA, United States of America

<sup>3</sup> Center for Theoretical Biological Physics, Northeastern Univ., Boston, MA 02115, United States of America

\* Author to whom any correspondence should be addressed.

<sup>4</sup> Current address: School of Mechanical Engineering, Tel Aviv University, Tel Aviv 69978, Israel.

E-mail: [kessler@dave.ph.biu.ac.il](mailto:kessler@dave.ph.biu.ac.il) and [levine.herbert@northeastern.edu](mailto:levine.herbert@northeastern.edu)

**Keywords:** notch/delta, signalling, patterns

## Abstract

Many developmental processes in biology utilize notch–delta signaling to construct an ordered pattern of cellular differentiation. This signaling modality is based on nearest-neighbor contact, as opposed to the more familiar mechanism driven by the release of diffusible ligands. Here, exploiting this ‘juxtacrine’ property, we present an exact treatment of the pattern formation problem via a system of nine coupled ordinary differential equations. The possible patterns that are realized for realistic parameters can be analyzed by considering a co-dimension 2 pitchfork bifurcation of this system. This analysis explains the observed prevalence of hexagonal patterns with high delta at their center, as opposed to those with central high notch levels (referred to as anti-hexagons). We show that outside this range of parameters, in particular for low *cis*-coupling, a novel kind of pattern is produced, where high delta cells have high notch as well. It also suggests that the biological system is only weakly first order, so that an additional mechanism is required to generate the observed defect-free patterns. We construct a simple strategy for producing such defect-free patterns.

## 1. Introduction

Biological cells can exist in a number of distinct phenotypes, even with a fixed genome. These phenotypes arise via multi-stability of the underlying dynamical network controlling cell behavior and allow cells to take on differentiated roles in overall organism function. It is clear that developmental processes must ensure that these phenotypes arise in the right place and time, i.e., ensure the emergence of functional phenotypic patterns.

A well-studied case of such a system is that of notch–delta signaling [1]. Various cells contain notch transmembrane receptors [2] that couple to notch ligands such as delta or jagged on both the same cell (*cis*-coupling) and neighboring cells (*trans*-coupling). Because of the manner by which notch and delta inhibit each other (see below), their interaction typically leads to an alternating ‘salt and pepper’ structure. This type of patterning is seen in systems ranging from eyes [3] and ears [4] to intestines [5] and livers [6]. An example of such a pattern is shown in figure 1 and for a review, see [7, 8]. As a general rule, the high delta cells are the most specialized ones (for

example, the photoreceptors [9]) and are surrounded by less differentiated high notch supporting cells—in what follows, these will be called hexagonal patterns. Parenthetically, changes in the transcriptional regulation utilizing the jagged ligand in place of delta may be crucial for the role of notch in cancer metastasis [10, 11], but here we focus solely on delta and its interplay with notch.

Patterning in the notch–delta system has been intensely studied [14–20], but questions remain regarding the relationship of the different nonlinear patterns seen and the role of the approximately hexagonal cell-layer geometry. There are also questions regarding the patterning accuracy, which in some systems can be very high; for example, the chances of getting two neighboring bristles (i.e. neighboring high delta cells) in the case of *Drosophila* is estimated to be less than 1% [21]. Also, the separation between high delta cells seems to vary between systems; not all cases look like the minimal pattern seen in the above figure. These questions persist at least partially due to the fact that even solving for the uniform state of the system cannot be performed analytically. In addition, the parameter space is quite large, even after

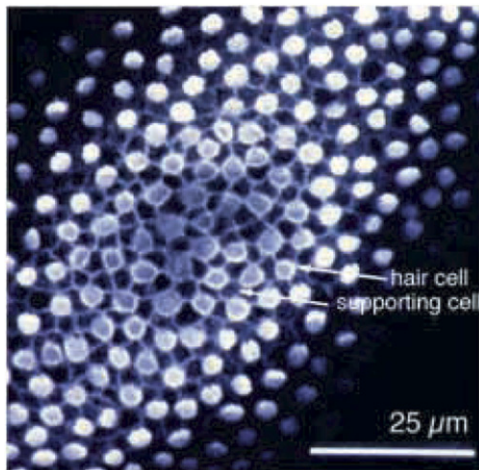


**Figure 1.** A regular alternating pattern of hair cells (bright tufts) and supporting cells (outlined by their cortical actin). Reproduced with permission from [12]. CC BY 4.0.

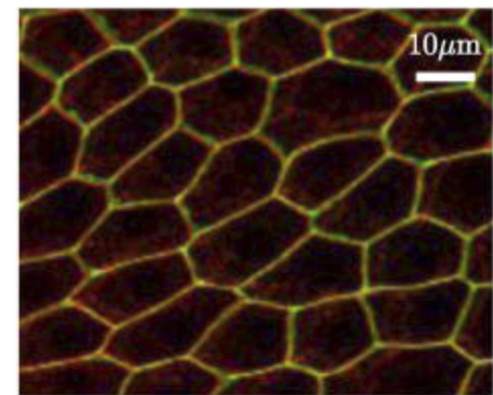


**Figure 2.** Epithelial layer of cells from the folical epithelium of Drosophila. Reproduced with permission from [13]. © IOP Publishing Ltd. All rights reserved.

dimensional reduction. The approach we adopt here is to perform a semi-analytical study, finding bifurcation points numerically and performing the nonlinear analysis around these points exactly. We combine this with extensive numerics to translate the bifurcation findings to the rest of the parameter space.

In this paper, we study the notch–delta system on a 2d hexagonal array of cells. The motivation for this choice is that epithelial layers consist of polygonal cells that roughly form a hexagonal lattice, albeit with some size dispersion and some defects (see figure 2). It is worthwhile to first work out how pattern formation works in the more idealized case of the perfect lattice and then afterwards consider possible effects of the irregularities; we do note in passing that some effort has already been devoted to understanding the role of variations in cell size [22]. We first focus on the existence and stability of hexagonal patterns in this geometry, which allows an exact re-writing of the (ordered) pattern-forming problem as a nine-dimensional dynamical system. We numerically construct the phase diagram of the system, showing the variety of patterns that emerge. Many features of this system can be understood by expanding about a co-dimension two pitchfork bifurcation. Others can be captured by examining various limiting cases of the parameters. The second focus of our work is mechanisms for ordered patterns to emerge from generic initial conditions. Here we identify a possible role for an initiating wave, similar to what has been seen in at least some biological realizations [23].

The notch–delta interaction is an example of juxtacrine (i.e., contact-dependent) signaling. As sketched in figure 3, ligands such as delta bind notch receptors and, when this occurs between neighboring cells, it leads to the cleavage of the receptor and release of its intracellular domain (NICD). NICD translocates to the nucleus where it transcriptionally

up-regulates notch and down-regulates delta. The ligand–receptor interaction between molecules on the same cell leads to mutual annihilation with no NICD release [15]. The combination of *cis*-annihilation and NICD-mediated trans-repression is responsible for the observed lateral inhibition of delta [14]. We will use a baseline model [18] of this process involving three concentrations,  $N$  (receptor),  $D$  (ligand) and  $I$  (NICD),

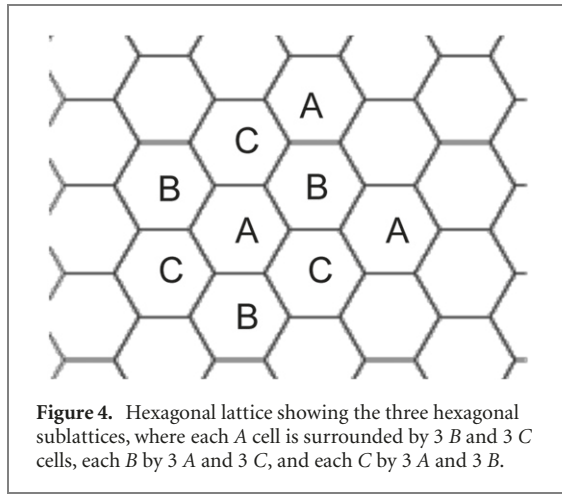
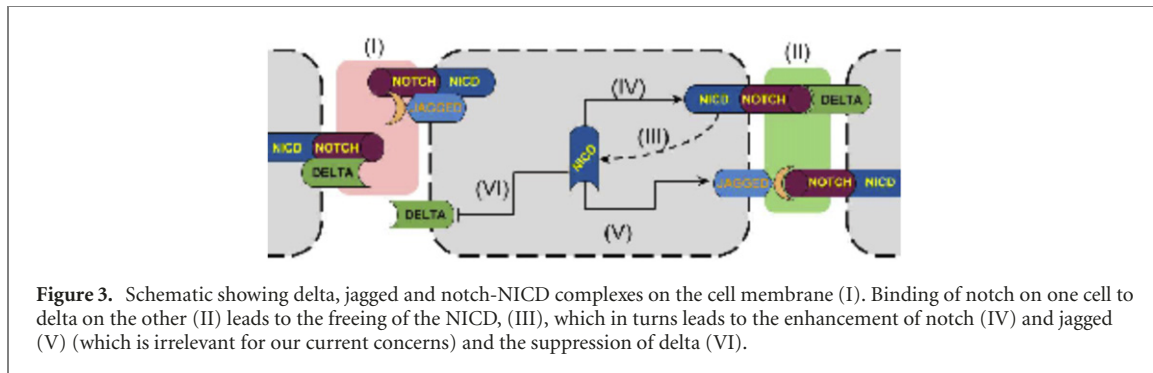
$$\begin{aligned}\dot{N}_x &= \lambda_N H_+(I_x) - N_x (k_c D_x + k_t D_x^{\text{ext}}) - \gamma N_x \\ \dot{D}_x &= \lambda_D H_-(I_x) - D_x (k_c N_x + k_t N_x^{\text{ext}}) - \gamma D_x \\ \dot{I}_x &= k_t \lambda_I N_x D_x^{\text{ext}} - \gamma_I I_x.\end{aligned}\quad (1)$$

Here, positions  $x$  refer to locations on an hexagonal lattice (see figure 4) and the superscript ‘ext’ refers the average over the six nearest neighbor sites of  $x$ . The production terms  $H_{\pm}$  corresponding to the aforementioned transcriptional regulation are taken to be Hill functions,

$$H_+(I) = 1 + \frac{k_H I^{n+}}{I^{n+} + s_0^{n+}}; \quad H_-(I) = \frac{s_0^{n-}}{I^{n-} + s_0^{n-}} \quad (2)$$

such that  $H_{\pm}(0) = 1$  and  $H_+$  is an increasing function that saturates at  $1 + k_H$ , while  $H_-$  is a decreasing function that decays to 0 with increasing  $I$ . We define a typical set of parameters taken from the literature [24]:  $\gamma = 0.1$ ,  $\gamma_I = 0.5$ ,  $n_+ = n_- = 2$ ,  $k_c = 0.1$ ,  $k_t = 0.04$ ,  $\lambda_I = 1$ ,  $k_H = 1$ ,  $s_0 = 1$ , and primarily focus on the role of  $\lambda_N$  and  $\lambda_D$ . Nevertheless, we will also have occasion to investigate the effects of changing  $k_H$  and  $k_t$ .

The outline of the rest of this paper is as follows. We first focus on uniform non-patterned solutions so that we can identify regions of parameter space in which these solutions become unstable. Because we work on a hexagonal lattice, mimicking the actual biological cell geometry, the first instability is to patterns with hexagonal symmetry and we show that these can be studied by an exact ODE reduction of



the spatially-extended model. We derive the general nature of the bifurcation and point out the relevance of a specific co-dimension two point at which there is an accidental symmetry between two families of solutions, which we call ‘hexagons’ and ‘anti-hexagons’, distinguished by the overexpressed (compared to the uniform state) species in the central hexagons of the honeycomb lattice comprising the pattern. We then construct the weakly nonlinear amplitude equation describing the system in the neighborhood of this special point and compare the results of our model with a simplified one-field version for which the accidental symmetry is replaced by a full symmetry of the non-linear system. We then consider ‘exotic’ solutions with overexpression of both notch and delta in the central cells. Lastly we consider how one might solve the problem of inhibiting defect formation. Algebraic details are left to appendices so as not to interfere with the flow of the manuscript.

## 2. Uniform patterns and the region of instability

We start by considering the simplest type of solution for this system of equations, namely one which is spatially uniform. In general, solving for such a solution requires the simultaneous solution of three nonlinear equations for  $N_0$ ,  $D_0$  and  $I_0$ . In appendix A, we show that one can reduce the problem to the solution of

one rather complicated equation for  $I_0$ ; this is given as equation (A5). For general values of the parameters, this last equation must be solved numerically.

We can gain some analytic insight into the solution space by considering various limiting cases (for full details see appendices B and C). One convenient such case is that of large  $\lambda_D$ . In that limit, we expect  $D_0$  to be large, which then forces  $N_0$  to be small to satisfy the condition arising from the last of equation (1),

$$k_t \lambda_I N_0 D_0 = \gamma_I I_0.$$

From the notch equation, we have in this limit

$$N_0 = \frac{\lambda_N H_+(I_0)}{(k_c + k_t) D_0}$$

which then immediately leads to the condition

$$I_0 = \mathcal{R}(I_0) \equiv \frac{k_t \lambda_N \left( 1 + k_H \frac{I_0^2}{1+I_0^2} \right)}{\gamma_I k_0}, \quad (3)$$

with  $k_0 \equiv k_c + k_t$  and where we have specialized to the case of Hill functions with  $n_{\pm} = 2$ . From this equation we can determine when there is a unique solution versus when multiple solutions exist. The details of this calculation are presented in appendix D. For our purposes here, we note that the range of parameters for which there is a unique uniform solution ranges over all reasonable values of the system parameters.

We are interested here in hexagonal patterns on our hexagonal lattice. These patterns arise as the uniform state becomes unstable with respect to spatially varying perturbations. In fact, our numerical experiments on equation (1) indicate that the first instability of the uniform state for the set of parameters above is almost always to a hexagonal mode, as that arrangement maximizes the average number of ‘satisfied’ nearest neighbor inhibitory interactions. This is of course a consequence of studying the model on a hexagonal grid, as motivated by the biological application. Then, the immediate question is where in parameter space the uniform state is unstable to a hexagonal pattern. The condition for this is presented in equation (A7) in appendix A. Similar calculations for other models of the notch–delta dynamics have been performed by Formosa-Jordan *et al* [16, 25] and

Negrete and Oates [20], and harken back to the original stability calculation for a two cell system by Collier *et al* [14]. The region of instability in the  $k_t$ ,  $\lambda_D$  plane is presented for various values of  $\lambda_N$ , both for  $k_H = 2/3$  in the left panel of figure 5 and for  $k_H = 4/3$  in the right panel. For each value of  $\lambda_N$  considered, the unstable region is that above the corresponding curve, i.e.  $\lambda_D > \lambda_D^c(k_t)$ . For each value of  $\lambda_N$ , the value of  $\lambda_D^c$  diverges at two values of  $k_c$ , with the instability only possible between these two values. For  $k_H = 2/3$ , the curve  $\lambda_D^c(k_t)$  doubles back on itself for low  $k_t$ , but not near the upper limiting value of  $k_c$ , whereas for  $k_H = 4/3$ , this doubling back happens on both sides. This qualitative change in behavior is explained in appendix C, and occurs at  $k_H = 1$ . Clearly whenever there is a hexagonal instability, a hexagonal solution exists. However, as we shall see, there is also the possibility of coexistence of a stable uniform solution with a hexagonal solution, so that hexagonal solutions extend outside the region of linear instability of the uniform state.

### 3. Hexagonally ordered patterns

We now turn to the construction of hexagonally ordered patterns whose existence (but not stability) is guaranteed by the linear instability discussed above. These patterns are invariant under translation with vectors  $\pm 6\hat{x}$ ,  $\pm 3\hat{x} \pm 3\sqrt{3}\hat{y}$  where  $\hat{x}$  and  $\hat{y}$  are unit vectors along the coordinate axes and the unit of length is 1/2 the length of one of the hexagonal sides. From figure 4, it is clear that the fields everywhere are completely determined by their values on three sub-lattices that we have labeled A, B and C. This means that the entire problem of hexagonally ordered patterns (and their stability with respect to modes invariant under translation of the A–B–C unit cell) is reduced to nine coupled ODE's. A mapping of the dynamics to a two-sublattice system, where the fields are equal on the B and C sublattices was used by Formosa-Jordan and collaborators to study the existence of perfect hexagonal patterns in references [16, 25]. The more complete three sublattice reduction was used in references [20, 25].

This exact mapping is very different than what occurs for more traditional pattern formation problems [26], such as convection rolls [27], where the reduction to a set of ODE's is valid only as an approximation near the bifurcation point. In the usual case, the challenge of finding non-linear solutions with high numerical accuracy and evaluating their stability can be quite challenging. Here by contrast, the above methodology enables the analysis to be accomplished in a relatively straightforward manner even far from the region of the bifurcation. As already shown, at fixed  $\lambda_N$ , the uniform solution with the fields taking on the same values on all three sublattices becomes unstable for  $\lambda_D > \lambda_D^U(\lambda_N)$  via a transcritical bifurcation, i.e. an intersection with a nonuniform solution.

On this new branch, the respective values of the fields on two sublattices (say B and C) are identical, differing from the values on the remaining (in this case, A) sublattice. This hexagonally structured solution has a six-fold hexagonal symmetry about any site on the different (here, A) sublattice. The bifurcation is transcritical in general, because of the lack of any symmetry between positive and negative deviations of the fields from their uniform values. As already mentioned and unlike convection, the transition to rolls does not take place at the same parameter value as that to hexagons as the roll pattern necessarily has a different wavelength on the lattice; hence rolls do not compete with hexagons, at least near the bifurcation. For completeness, the six coupled equations that govern ordered hexagonal patterns are given explicitly in appendix E.

### 4. The pitchfork bifurcation and its unfolding: the Negrete–Oates model

To understand the nature of the origin of hexagonal patterns in a hexagonal lattice system, Negrete and Oates [20] introduced a simple one-field model containing the same type of instability. The model is given by

$$\dot{u}_n = -u_n - \gamma u_n^3 + \Omega_0 + \epsilon u_{\text{ext}}, \quad (4)$$

where again  $u_{\text{ext}}$  is the average of  $u$  on the six nearest-neighbor sites. For sufficiently negative  $\epsilon$ , this model has a lattice analog of a negative diffusion constant and hence become unstable to hexagonal patterns. On the three sites of the unit cell introduced above, this system reduces to

$$\begin{aligned} \dot{A} &= -A - \gamma A^3 + \Omega_0 + \epsilon(B + C)/2 \\ \dot{B} &= -B - \gamma B^3 + \Omega_0 + \epsilon(A + C)/2 \\ \dot{C} &= -C - \gamma C^3 + \Omega_0 + \epsilon(A + B)/2. \end{aligned} \quad (5)$$

They noted the presence of a pitchfork bifurcation at a specific value of the parameters, namely  $\epsilon_{\text{PF}} = -2$ ,  $\Omega_{\text{PF}} = 0$ . The latter is directly dictated by the symmetry  $u \leftrightarrow -u$  of their equations, which of course only is present at  $\Omega_0 = 0$ . The existence of this pitchfork bifurcation point guarantees the existence of two types of hexagonal patterns, which we call 'hexagons' (high delta surrounded by high notch) and 'anti-hexagons'. In the Negrete–Oates model [20], these two families of solutions are trivially related by  $u \rightarrow -u$  and  $\Omega \rightarrow -\Omega$ . As we shall see, in our three-field more biologically realistic model, the pitchfork point exists for a wide range of parameters, and again dictates the existence and stability properties of both families of solutions in the vicinity of the pitchfork point. However, as opposed to the Negrete–Oates model, this more detailed model does not exhibit an exact symmetry at the pitchfork point. Rather, the symmetry exists only to linear order and is broken at higher order. Nevertheless, given the relatively simple structure of the Negrete–Oates model, it is very useful

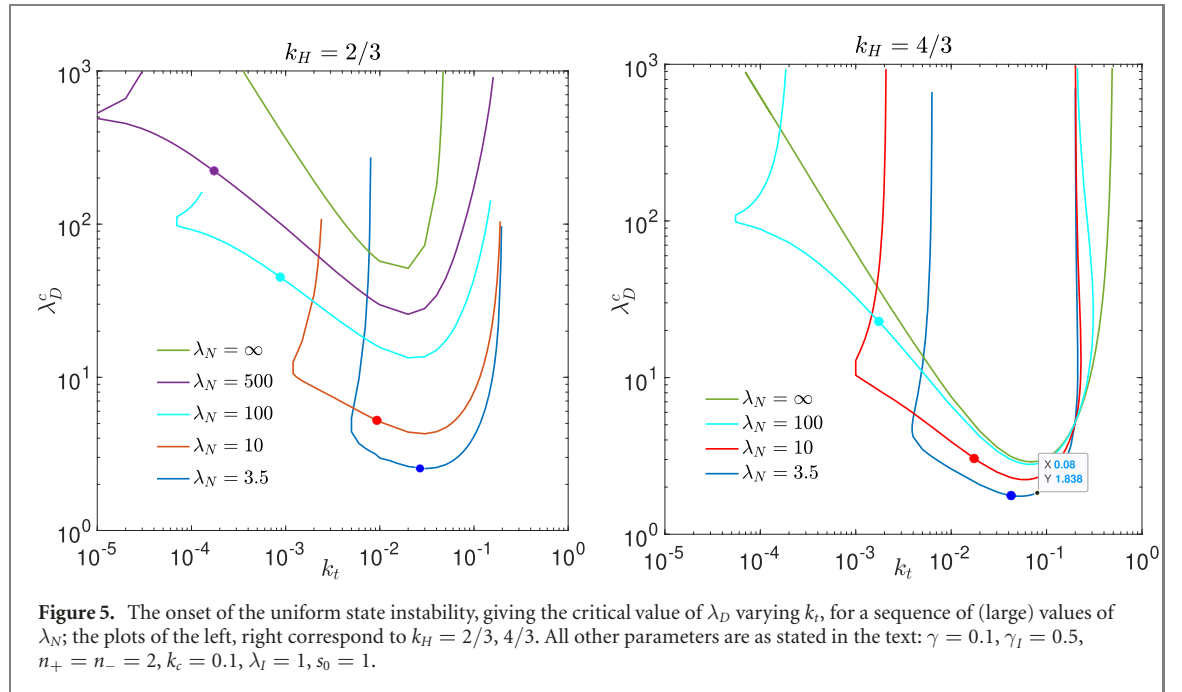


**Figure 5.** The onset of the uniform state instability, giving the critical value of  $\lambda_D$  varying  $k_t$ , for a sequence of (large) values of  $\lambda_N$ ; the plots of the left, right correspond to  $k_H = 2/3, 4/3$ . All other parameters are as stated in the text:  $\gamma = 0.1, \gamma_I = 0.5, n_+ = n_- = 2, k_c = 0.1, \lambda_l = 1, s_0 = 1$ .

to go through the exercise of working out the weakly nonlinear analysis (for an introduction to bifurcations and weakly nonlinear analysis, see [28]) for this model in the vicinity of the pitchfork point, as the overall algebraic structure of our three-field model is quite similar but significantly more complicated in detail.

The homogeneous stationary state  $A = B = C \equiv H$  satisfies

$$0 = -H - \gamma H^3 + \Omega_0 + \epsilon H \quad (6)$$

with solution  $H \approx \Omega_0/(1 - \epsilon)$  for small  $\Omega_0$ . At the critical value  $\epsilon_c = -2 - 6\gamma H^2$ , the stability matrix around the homogenous solution has two zero modes,  $(\delta A, \delta B, \delta C) = (-2, 1, 1)$  and  $(0, 1, -1)$  and the nonzero mode  $(1, 1, 1)$ , with eigenvalue  $-3$ . We will be carrying out a weakly-nonlinear analysis in the neighborhood of the co-dimension two pitchfork bifurcation point. To obtain this, we write

$$\begin{aligned} A &= H - 2C_1 + \delta_2 \\ B &= H + (C_1 + C_2) + \delta_2 \\ C &= H + (C_1 - C_2) + \delta_2, \end{aligned} \quad (7)$$

where  $C_1$  and  $C_2$  are the  $\mathcal{O}(\Omega_0)$  amplitudes of the zero modes, and  $\delta_2$  is an  $\mathcal{O}(\Omega_0)^3$  correction. Writing  $\epsilon = \epsilon_c + \Delta\epsilon$ , where  $\Delta\epsilon$  is  $\mathcal{O}(\Omega_0)^2$ , and expanding to third order in  $\Omega_0$ , we obtain three equations for the time-dependent amplitudes  $C_1$  and  $C_2$  (which vary on the slow time scale  $\Omega_0^2$ ) and  $\delta_2$ . Eliminating  $\delta_2$ , we find the two amplitude equations

$$\begin{aligned} \dot{C}_1 &= \frac{-C_1 \Delta\epsilon}{2} - 3\gamma C_1^3 - \gamma C_1 C_2^2 + \gamma H(3C_1^2 - C_2^2) \\ \dot{C}_2 &= \frac{-C_2 \Delta\epsilon}{2} - \gamma C_2^3 - 3\gamma C_1^2 C_2 - 6\gamma H C_1 C_2, \end{aligned} \quad (8)$$

where the time derivatives refer to variation on the aforementioned slow time scale. It is easy to see that all the terms in our equations are  $\mathcal{O}(\Omega_0)^3$ .

We start by looking for time-independent solutions of these equations. One stationary state of the system is the original homogeneous state with  $C_1 = C_2 = 0$ . There is a pair of solutions with  $C_2 = 0$ , with  $C_1$  satisfying the quadratic equation

$$0 = -\frac{\Delta\epsilon}{2} + 3\gamma H C_1 - 3\gamma C_1^2. \quad (9)$$

These two solutions emerge from a saddle-node bifurcation occurring at  $C_1 = H/2, \Delta\epsilon = 3\gamma H^2/2$ . This lies on the stable side of the transition and thus the saddle node bifurcation precedes the instability of the homogenous state as  $\epsilon$  is decreased. As  $\Delta\epsilon$  further decreases from its saddle-node value, one of the solution branches has increasing  $C_1$ , while the other approaches  $C_1 = 0$ , i.e., the homogeneous solution, intersecting it at  $\Delta\epsilon = 0$ , the location of the homogeneous instability. It then crosses over to  $C_1 < 0$ , so that here it has ‘polarity’ opposite to that of the other branch emerging from the saddle-node bifurcation that had  $C_1 > 0$  and increasing.

There are other stationary solutions, having  $C_2 \neq 0$ . Solving the  $\dot{C}_2 = 0$  equation for  $C_2$  and substituting in the  $\dot{C}_1 = 0$  equation yields  $C_1 = -x/2$ , where  $x$  is the value obtained above for  $C_1$  when  $C_2 = 0$ . Substituting this back into the equation for  $C_2$  then reveals  $C_2 = \pm 3x/2$ . For these solutions, the leading order value of  $A - H$  is  $-2C_1 = x$ , which was the leading order value of  $B - H = C - H$  in our original solution. In addition, either  $B - H$  or  $C - H$  (depending on the sign of  $C_2$ ) equals  $x$  as well, with the other equalling  $-2x$ , which was the value of  $A - H$  in the original solution. Thus, all these new solutions are simply the previous solutions translated to

be centered on  $B$  or  $C$ , instead of  $A$ . At the linear level, these new solutions are the linearly combinations  $-1/2[(-2, 1, 1) \pm 3(0, 1, -1)]$  of the two zero modes of the homogeneous solution. This crossing of this inhomogeneous solutions with the original homogeneous solution represents a two dimensional transcritical bifurcation of the homogeneous solution; two-dimensional here because of the two zero modes of the homogeneous solution. Precisely at  $\Omega_{\text{PF}}$ , i.e.,  $\Omega_0 = 0$ , the saddle node merges with the transcritical point and the two branches meet symmetrically at  $\Delta\epsilon = 0$ , i.e.,  $\epsilon_{\text{PF}}$ , as indicated by the vanishing of the term linear in  $C_1$  in equation (9).

We can also easily calculate the stability spectrum of the non-trivial patterned states of this reduced system. The homogeneous solution has a degenerate pair of modes, with growth rates  $\Omega_1 = \Omega_2 = -\Delta\epsilon/2$ , so that is stable below the transition,  $\Delta\epsilon > 0$  and unstable above. Focusing on the  $C_2 = 0$  inhomogeneous solution, it has two eigenvalues,  $\Omega_1 = 3\gamma C_1 (H - 2C_1)$  and  $\Omega_2 = -9\gamma C_1 H$ . From this we can see that (for  $\Omega_0 > 0$ ) on the positive branch both modes are stable.  $\Omega_1$  crosses 0 at the saddle node, and on the second branch we have 1 stable and one unstable mode. When the second of the non-uniform branches crosses the homogeneous solution at the transcritical point, both  $\Omega$ 's cross zero and we remain with one stable and one unstable mode, switched compared to those on the previous side. The story for the other, shifted, solutions is of course the same. This picture is more intricate than for the standard co-dimension one pitchfork, where the stable solution on one side of the bifurcation gives rise to one unstable and two symmetry-related stable solutions on the other side.

## 5. The pitchfork bifurcation and its unfolding: the biological notch–delta model

Numerical exploration of equation (1) confirms that our more realistic notch–delta system also possesses a co-dimension 2 pitchfork bifurcation over a wide range of parameters. For our standard parameters, the pitchfork occurs at  $\lambda_N^{\text{PF}} = 2.758\,2488$ ,  $\lambda_D^{\text{PF}} = 1.931\,12$ . Specifically, for  $\lambda_N^{\text{PF}}$ , as is the case for general  $\lambda_N$ , only the uniform solution exists for  $\lambda_D < \lambda_D^U$  and it is stable. At  $\lambda_D^U = 1.931\,12$ , two additional solutions are born, one a ‘hexagon’ (by definition, a solution where high  $D$  is surrounded by high  $N$ ) and one an ‘anti-hexagon’ (high  $N$  surrounded by high  $D$ ). What is interesting is that this point occurs not only for physically possible (i.e. positive) values of the parameters, but within the range of parameter values determined (at least roughly) by experiment [15]. Thus the unfolding of the bifurcation gives us detailed information about the pattern formation possibilities realizable in real physiological settings.

Many of the features in the vicinity of the pitchfork bifurcation of the Negrete–Oates model carry

over into our more complicated system. Specifically, it can directly be shown by numerical analysis of the nine-dimensional reduced system that the uniform state has 2 (degenerate) unstable modes above the critical  $\lambda_D$ . The emerging hexagon branch is stable, whereas the anti-hexagon has one unstable mode. The instability is with respect to a mixed mode (defined as a mode with all three sublattices having different values) which converts the anti-hexagon to a shifted hexagon. This overall structure is shown in figure 6(A), and indeed recapitulates the structure determined for the Negrete–Oates model via the amplitude equation analysis.

At all other values of  $\lambda_N$ , the pitchfork breaks up into a transcritical bifurcation and a saddle-node (see figure 6(B)), also as in the Negrete–Oates model. Again by direct numerical solution, we find that for  $\lambda_N > \lambda_N^{\text{PF}}$ , the uniform solution undergoes a transcritical bifurcation with an unstable anti-hexagon (with respect to a mixed-mode perturbation) on the high  $\lambda_D$  side and an unstable (with respect to a pure-mode) hexagon on the low  $\lambda_D$  side. The unstable hexagon then undergoes a saddle-node bifurcation, rendering the hexagon stable; this stable branch then continues on as  $\lambda_D$  increases. For  $\lambda_D$  smaller than the saddle-node value, no patterned solution exists. Hence, there exists a range of parameters for which a stable hexagon coexists with the stable uniform solution, a range which widens as  $\lambda_N$  increases; we will return to this point below. For example, for  $\lambda_N = 3.5$ , the transcritical bifurcation in which the uniform state goes unstable is at  $\lambda_D = 2.113\,56$ , whereas the saddle node bifurcation is at  $\lambda_D = 2.1097$ . An example of a stable hexagon solution for  $\lambda_N = 3.5$ ,  $\lambda_D = 2.3$  is shown in figure 7.

A similar bifurcation structure appears for  $\lambda_N < \lambda_N^{\text{PF}}$ , where now the stable hexagon lies to the right of the transcritical point and the unstable anti-hexagon lies to the left, and it is the one that undergoes a saddle-node bifurcation (see figure 8(A)). The anti-hexagon is born with 1 unstable mode at the transcritical point and turns stable at the saddle-node bifurcation. However, unlike what happened in the Negrete–Oates model [20], the stable anti-hexagon branch loses stability to a mixed-mode perturbation; this instability leads to a new pitchfork bifurcation, which is a result of the  $B/C$  symmetry breaking. The hexagon, on the other hand, is born with one unstable mode and subsequently becomes stable, also as a result of a mixed-mode pitchfork bifurcation. An overall diagram of the stable phases as a function of the two parameters  $\lambda_N$  and  $\lambda_D$  is presented in figure 8(B). The mixed-mode solution branch arising from the hexagon bifurcation is the same solution which arises from the anti-hexagon bifurcation. For example, at  $\lambda_N = 2$ , the hexagon becomes stable at  $\lambda_D = 2.0477$  and the anti-hexagon becomes unstable at  $\lambda_D = 2.056$ . Thus, there is a very small coexistence region between the hexagon and

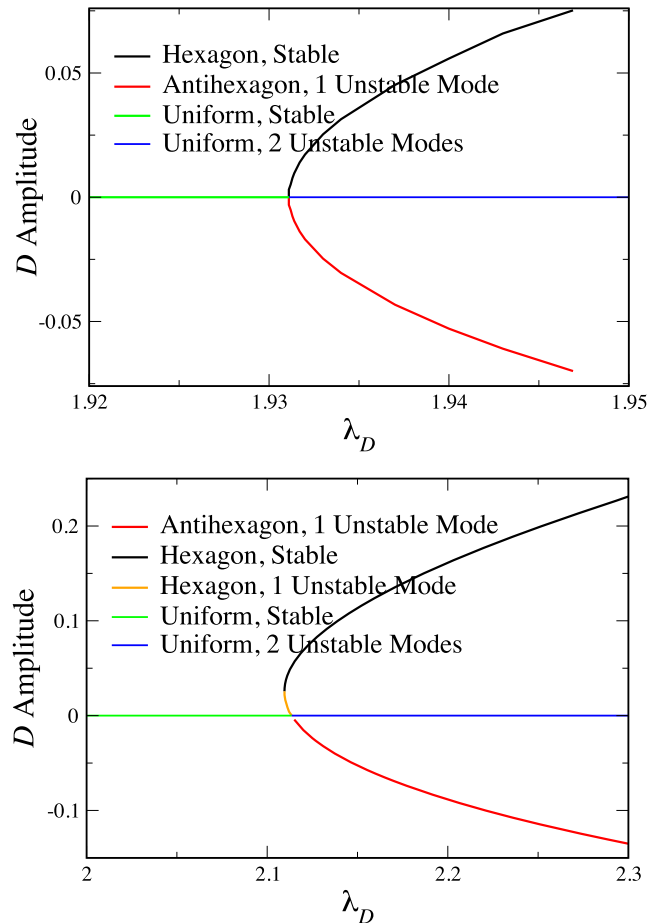


**Figure 6.** Bifurcation diagrams: (A) for the critical  $\lambda_N^{PF} = 2.758\ 2488$  for which there is a pitchfork bifurcation; (B) for  $3.5 = \lambda_N > \lambda_N^{PF}$  where there is an imperfect bifurcation. All other parameters are standard.

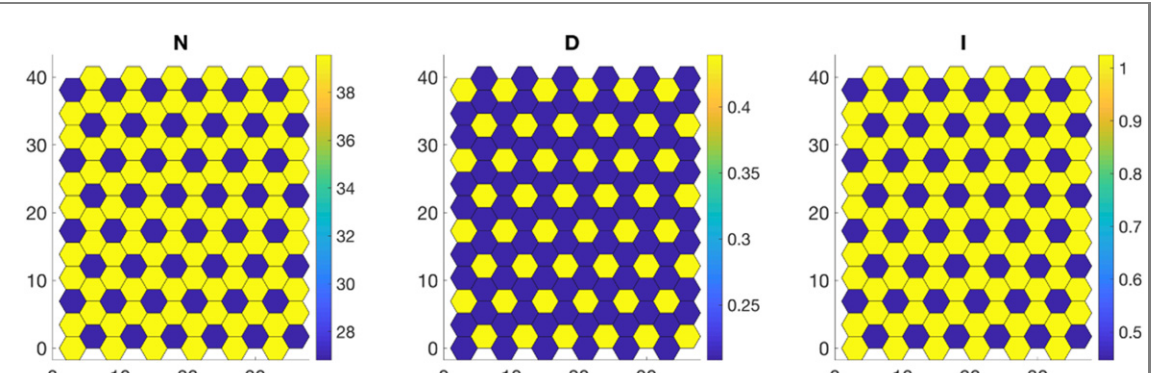


**Figure 7.** A stable hexagon solution for  $\lambda_N = 3.5$ ,  $\lambda_D = 2.3$ . All other parameters are standard.

anti-hexagon solutions. Again, the only solution that survives stably to higher values of  $\lambda_D$  is the hexagon. This is in accord with the general biological rule given above that the high delta cells are surrounded by high notch cells sufficiently far from  $\lambda_N^{PF}$  and its associated  $\lambda_D^U$ . From the physics perspective, the explicit lack of symmetry between notch and delta as reflected in this model is not eliminated by working close to the co-dimension two bifurcation since the accidental symmetry at this point affects only the leading order term in the amplitude equation, not

any of the higher-order ones. As mentioned above, this feature is not captured by the simpler one-field model where the model has an exact symmetry at  $\Omega_0 = 0$ .

We can again use weakly non-linear bifurcation theory to flesh out these numerical findings, working in the immediate vicinity of the pitchfork bifurcation, the bifurcation analysis for this more complicated system of nine equations can be performed, and after eliminating the seven fast modes (as opposed to just one previously), we get a set of amplitude

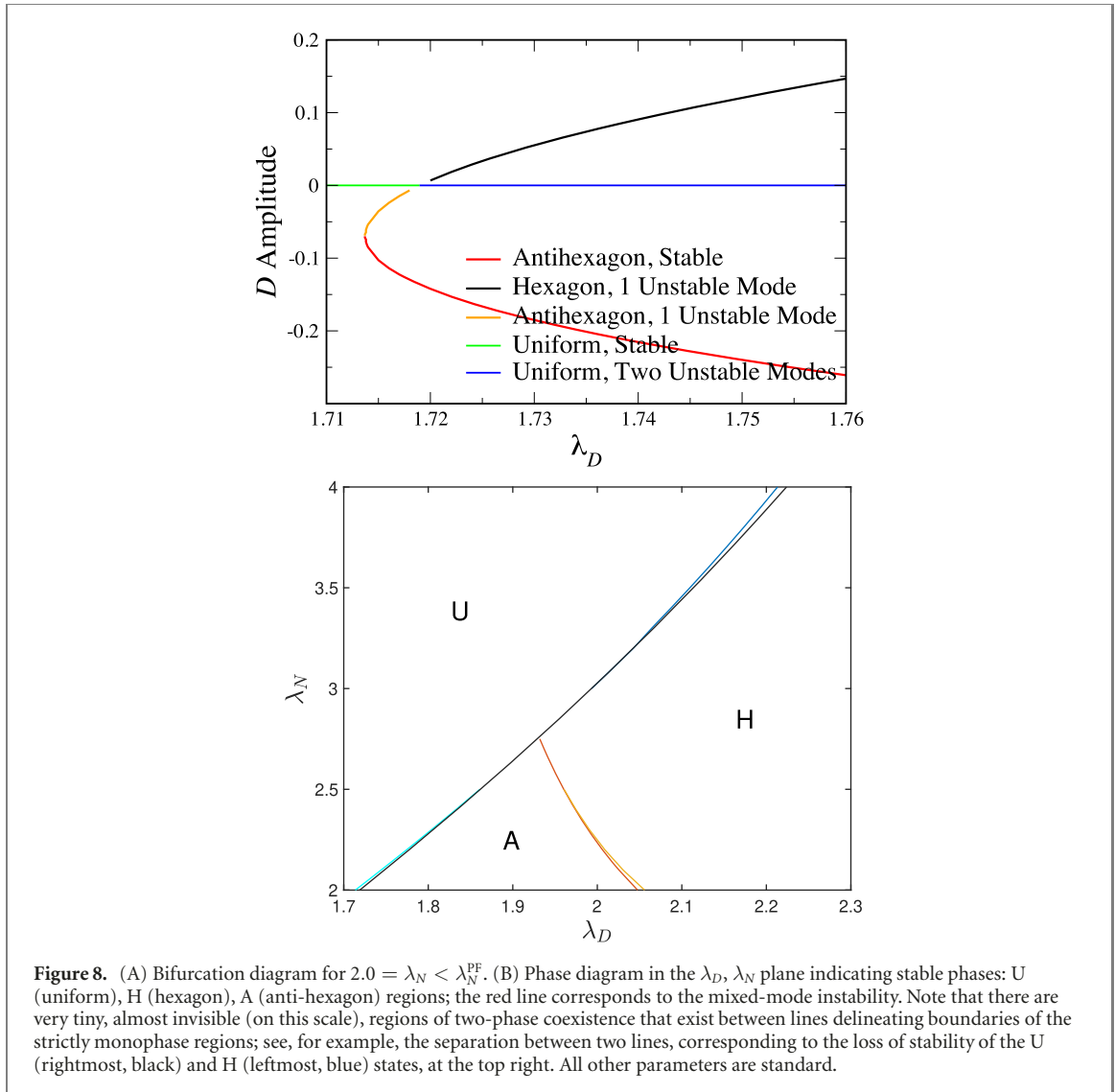


**Figure 8.** (A) Bifurcation diagram for  $2.0 = \lambda_N < \lambda_N^{\text{PF}}$ . (B) Phase diagram in the  $\lambda_D, \lambda_N$  plane indicating stable phases: U (uniform), H (hexagon), A (anti-hexagon) regions; the red line corresponds to the mixed-mode instability. Note that there are very tiny, almost invisible (on this scale), regions of two-phase coexistence that exist between lines delineating boundaries of the strictly monophase regions; see, for example, the separation between two lines, corresponding to the loss of stability of the U (rightmost, black) and H (leftmost, blue) states, at the top right. All other parameters are standard.

equations for the two slow modes, parameterized by  $\delta_{B,C} = N_{B,C} - N_0$ , where  $N_0$  is the homogeneous notch level. Doing this, we get exactly the same bifurcation equations structure as in equation (8) with the role of the symmetry breaking parameter  $\Omega_0$  played by  $\delta \equiv \lambda_N - \lambda_N^{\text{PF}}$  and the role of the other bifurcation parameter  $\Delta\epsilon$  replaced by  $\epsilon \equiv (\lambda_D - \lambda_D^{\text{c}})$  where  $\lambda_D^{\text{c}}$  is the location of the instability of the homogeneous solution. Near  $\lambda_N^{\text{PF}}$ ,

$$\lambda_D^{\text{c}} \approx 1.931 + 0.262\delta - 0.0236\delta^2 + 0.000676\delta^3 \quad (10)$$

so that  $\lambda_D^{\text{c}}$  increases with  $\lambda_N$ . We can write the final amplitude equations as

$$\begin{aligned} \dot{C}_1 &= \alpha C_1 + \sigma(3C_1^2 - C_2^2) + \mu C_1(3C_1^2 + C_2^2) \\ \dot{C}_2 &= \alpha C_2 - \sigma(6C_1C_2) + \mu C_2(C_2^2 + 3C_1^2). \end{aligned} \quad (11)$$

In term of these bifurcation parameters  $\delta$  and  $\epsilon$ , the amplitude equation coefficients are

$$\alpha = 0.04440\epsilon; \sigma = 0.000382\delta; \mu = -0.0003063. \quad (12)$$

This system is of course identical in structure to that we received in the Negrete–Oates model. The new information is the connection of the perturbations  $C_1, C_2$  to the deviations from homogeneity of the physical fields  $N, D$ , and  $I$ .

The analysis of these equation thus follows directly from our previous analysis. Here, the saddle-node point is at  $\epsilon = -0.00807\delta^2$ , again below the transition, with  $C_1^{\text{SN}} = 0.6244\delta$ , so that for  $\delta > 0$  the  $B$  and  $C$  sites has high notch, so that the  $A$  site has low notch. From the solution for the fast modes, we have  $D_A = D_0 + 0.0276C_1$ , and the  $A$  site has high delta. Thus the saddle-node solution is what we entitle a ‘hexagon’ solution, which of course a distinction that is meaningless in the one-field model. On the other side of the transcritical point,  $C_1$  changes sign, and so the  $A$  site there has low notch and high delta, i.e. an anti-hexagon. For  $\delta < 0$ , i.e.  $\lambda_N < \lambda_N^{\text{PF}}$ , things are reversed, and the saddle node has  $C_1 < 0$ , so that the saddle-node solution is an anti-hexagon, and the solution on the other side of the transcritical point is a hexagon. This is of course consistent with our detailed numerical findings.

Checking the stability, both homogeneous modes have growth rate  $\alpha$ , and so are stable for  $\lambda_D < \lambda_D^c$  and unstable above the transition. For the  $\delta > 0$  hexagon, one mode, with growth rate  $\Omega_1$  is stable on the upper branch  $C_1 > C_{1,SN}$  and unstable for  $C_1$  below the saddle node. The other mode, with growth rate  $\Omega_2$  is stable both above and below the saddle node. Thus, the hexagon on the upper branch is stable and on the lower branch is once unstable. Across the transcritical point, the two modes switch signs, and the anti-hexagon also has one unstable mode. For  $\delta < 0$  on the other hand, the bottom antihexagon is stable and the top antihexagon and the hexagon are once unstable. Precisely at  $\lambda_N = \lambda_N^{PF}$ ,  $\Omega_1$  and  $\Omega_2$  both vanish and one has to go to higher order to see that the antihexagon is the unstable solution. Also, the instability of the anti-hexagon to the mixed mode is not present to this order of the amplitude equation analysis.

## 6. Exotic solutions

The aforementioned exact mapping of the ordered pattern equations to a coupled ODE system allows as well for the analytic understanding of a surprising type of pattern not heretofore investigated. If we solve our system at a low value of  $k_c = 10^{-4}$ , with  $\lambda_N = 3.5$ ,  $\lambda_D = 10$  and all other parameters at standard values, we find a hexagonal structure with  $N_A = 52.7 > N_B = 51.0$ , while as usual  $D_A = 0.558 > D_B = 0.215$ . We refer to this type of solution as ‘high-high’, as cells with high delta also have high notch (‘high’ here is relative to the neighboring cells). However, we did not find any evidence for this possibility over the range of *cis*-inhibition parameters proposed by Sprinzak, *et al* for typical developmental processes; this is shown in a numerically computed phase diagram (figure 9). This might explain why such patterns have not been seen experimentally to date. To better understand the phase diagram, we show in appendix F how one can analytically derive the boundary between regular hexagons and high-high solutions in the large  $\lambda_D$  limit. Specifically, an accurate approximation for the vertical line in the figure is  $k_c^* = k_t/2(1 + k_H)$ , which equals 0.01 with our typical choices. This result shows that hexagonal patterns are not dependent on having high *cis*-inhibition but that the anti-correlation between delta and notch cannot be taken for granted in its absence.

## 7. Initial value problem

The existence of stable ordered hexagons leaves open the question of how these patterns can be generated in the noisy biological system with plausible initial conditions [19, 29]. In particular, it is easy to check numerically that, starting with no pattern for a set of parameters for which the uniform state is linearly unstable, the presence of noise, either in the

initial data or in the time evolution, will lead to disordered states with many domain boundaries between hexagon patterns centered on different sublattices. One way out is based on the fact we have shown above that there could exist a parameter range for which there is a subcritical bifurcation to stable hexagons in which case a local perturbation which nucleates the pattern can spread in an ordered manner; this is a standard scenario in many non-living systems [26]. Crucially, the bifurcation analysis suggests that for biological systems studied to date, there is no significant range of physiologically relevant parameters where propagation would occur into a metastable state. Intuitively, we believe that most biological systems exhibit insufficient parameter control and too high a level of stochasticity for this to be a robust strategy. In some, coupling to additional components could alter the bistability range. There could also be more complex biological mechanisms that, for example, would provide downstream checks that prevent neighboring cells from both developing the same phenotype even if there is some initial defect in the notch–delta structure [30].

A more physics-based possibility is that the system is not put all at once into the unstable state. This possibility was examined by Formosa-Jordan and collaborators [25, 31], who introduced an additional morphogen field which served as a propagating precursor wave immediately behind which the system is found in the unstable homogeneous state. The primary focus of this earlier work was on the nature of the precursor wave and the finding of an instability of the wave pattern to transverse perturbations under certain conditions. In addition they noticed that the resulting pattern became more disordered as the wave spread increased, but did not systematically investigate this effect. To better understand this finding, we imagine that the system is initially in a regime of parameter space for which the uniform state is stable. Then some external mechanism (such as the morphogen dynamics above) induces a propagating wave, behind which the parameters are in the unstable region. To exhibit this possibility, we assume that only  $\lambda_D$  is affected by this wave, and  $\lambda_D = 2$  ahead of the wave and  $\lambda_D = 3.5$  behind the wave. For simplicity, we do not concern ourselves here with the origins or dynamics of this initiation wave, and rather choose a standard  $\tanh$  waveform, and vary the wave speed  $v$ . In figure 10, we show a pair of simulations of our model augmented by quenched noise. The wave in  $\lambda_D$  propagates radially outward from an initial point creating an expanding region inside of which the system exhibits notch–delta patterning. At large  $v$ , the parameter shift is essentially instantaneous over a large spatial region and the noise nucleates incommensurate patterns in different parts of the lattice, leading to obvious defects. If the parameter wave is slowed down, the leading edge of the pattern has sufficient time to align itself with the preceding rows

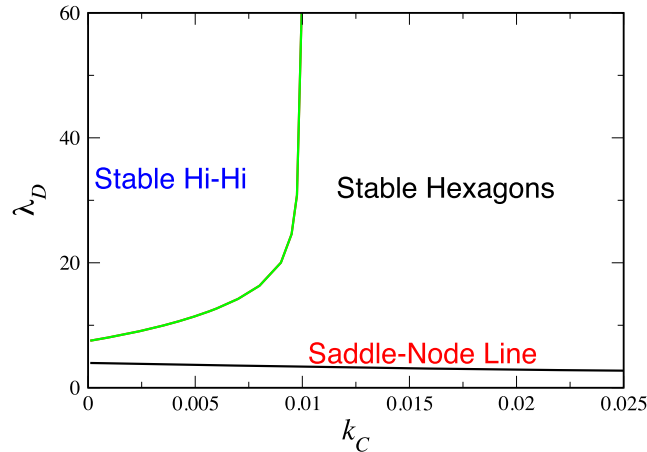


**Figure 9.** Phase diagram in the  $k_c$ ,  $\lambda_D$  plane showing the transition from the uniform state (low  $\lambda_D$ ) to hexagonal patterns (saddle-node line) as well as the smooth change from the normal to the high-high pattern.  $\lambda_N = 3.5$ . All other parameters standard.

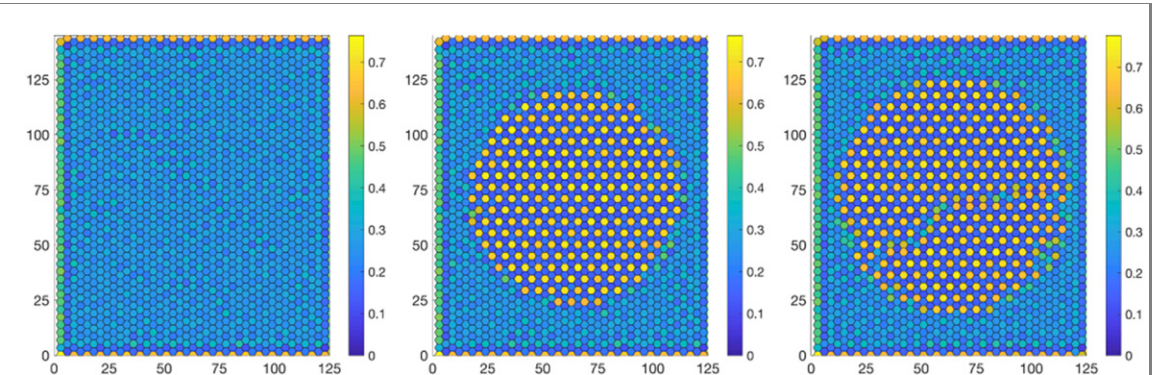


**Figure 10.** The pattern (of  $D$ , the patterns of  $N$  and  $I$  are similar) created by a radially propagating initiation wave raising  $\lambda_D$  from its initial value of 2 to a final value of 3.5. Left panel: the system before the arrival of the wave. The bulk variation in  $D$  is caused by a quenched 3 percent Gaussian variation in  $k_c$  from cell to cell. Middle panel: the ordered pattern resulting from a slow ( $v = 0.015 \text{ cells s}^{-1}$ ) initiation wave. Right panel: the multi-domain structure resulting from a fast ( $v = 0.05 \text{ cells s}^{-1}$ ) initiation wave.  $\lambda_N = 3.5$ . All other parameters were standard.

before having to itself act as a template for the next radial row. Therefore, any wave speed below a critical threshold would be sufficient to obtain the disorder reduction. An estimate of the speed of one such wave (the morphogenetic furrow during *Drosophila* eye development [32]) is well below this threshold. One can do this as well in a planar geometry, (where a linear front traverses the system from one side, see below), as is suggested by some biological data [3]. This scenario, in which the bistable dynamics is decoupled from the patterning dynamics, is an alternate route to constructing a model of the precursor wave than the above-mentioned morphogen dynamics, which is assumed to be driven by the developing pattern.

One extension of this analysis considers the fact that biological tissue will in general differ from perfectly hexagonal cellular organization [33]. To get some sense of the importance of this disorder, we have generated three lattice configurations, ranging

from small to moderate disorder as measured by the number of non-hexagonal cells. For comparison, we note that in many cases the measured number of hexagons is around 50% [33], although in some cases the percentage can be even smaller. These were generated using the continuous random network (CRN) approach [34, 35]; for details, see appendix G. In figure 11, we show (in this case for the planar geometry) that the precursor wave idea is still very effective at generating ordered structures. This finding can be seen directly by examining the  $D$  field patterns and can be quantitated by measuring the number of times two neighboring cells both exhibit high  $D$  values. A more detailed analysis of the effects of disorder will be presented elsewhere.

Parenthetically, the above approaches differ from the ideas presented in references [32, 33], there, they propose a templating mechanism for the production of the final ordered pattern and compare to data for the *Drosophila* eye system. Our approach,

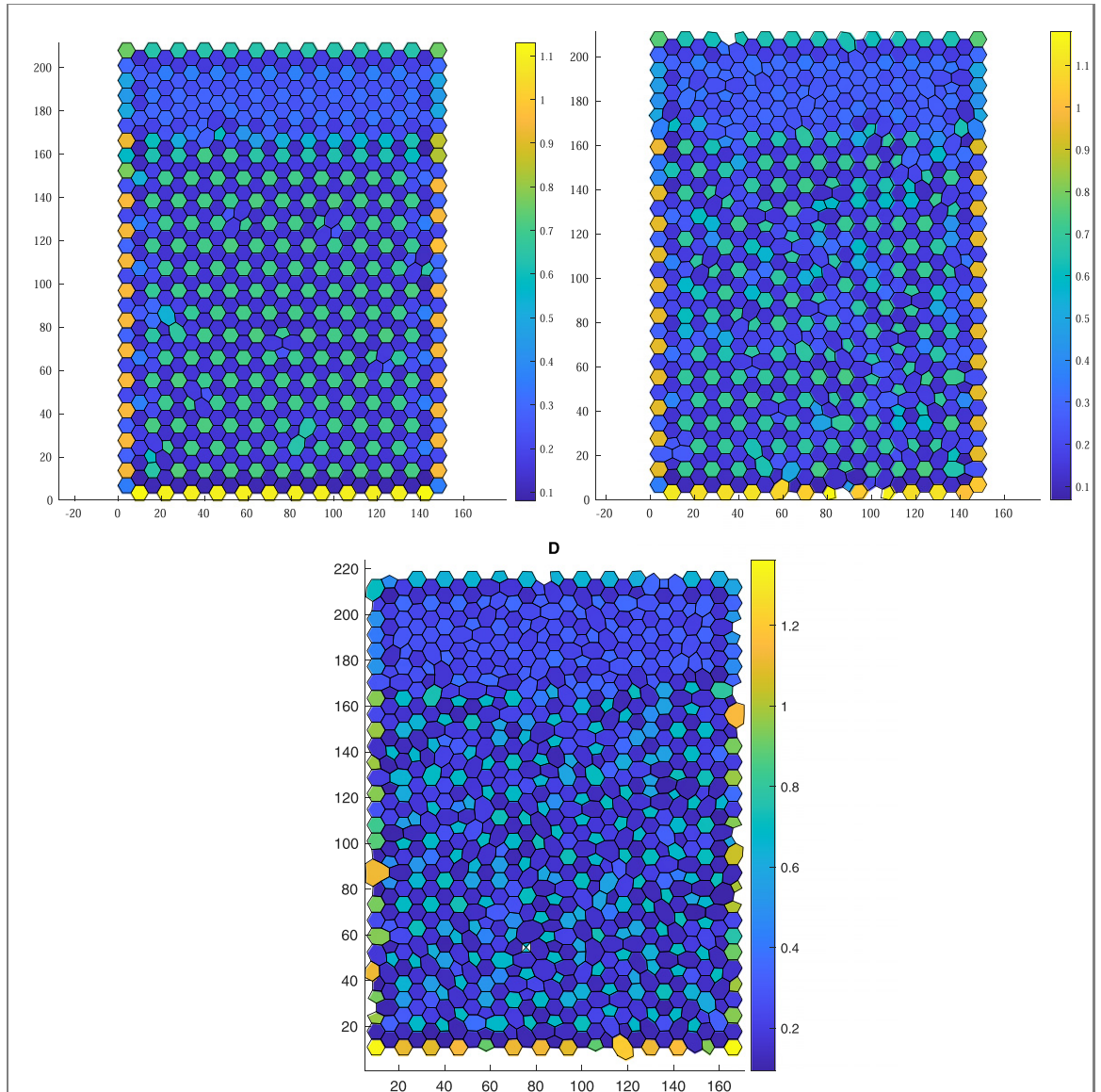


**Figure 11.** The pattern (of  $D$ , the patterns of  $N$  and  $I$  are similar) created by a linearly propagating initiation wave raising  $\lambda_D$  from its initial value of 2 to final value of 3. Left top panel: propagation into a system with roughly 10% non-hexagonal cells. We see that only in four instances are there pairs of adjacent cells with high  $D$  in the region completely passed over by the initiation wave. Right top panel: propagation into a more disordered system, with roughly 25% non-hexagonal cells. While there are more pairs of adjacent high- $D$  cells, the basic structure of high- $D$  cells surrounded by low- $D$  cells is preserved. Bottom panel: even with the number of hexagons equal to roughly 50%, the basic ‘salt and pepper’ pattern is maintained. The speed of the wave was  $0.01 \text{ s}^{-1}$ , where the lattice spacing is 4.  $\lambda_N = 3.5$ . All other parameters are standard.

on the other hand, builds on the known interaction in the notch–delta pathway and does not require a pre-patterned template. Another proposed solution involves the presence of carefully adjusted time-delays in the signalling network [19].

One last remaining pattern selection question concerns the fact that, in some systems, multiple less-differentiated cells separate the fully differentiated high delta ones. The pattern is still hexagonal but with a wavevector that is smaller than the maximum allowed by the lattice structure. Such patterns exist in our model, but would not be selected by any simple initial value problem. This is because as been shown here and elsewhere, the most unstable wavevector is the largest one, i.e. lies at the end of the Brillouin zone. Possible mechanisms could include the more

complex initial value templating of [33] or having the inhibition from the high delta cells extend beyond their nearest neighbors. Such an extension mechanism involving filopodial appendages was demonstrated by Cohen and co-workers [34]. A related possibility is coupling the notch–delta juxtracrine process to paracrine signaling, either by having some diffusible notch ligand (such as is known to occur for Jag1 [35]) or via coupling to a different molecular inhibitor. In all of these extended inhibition scenarios, it is easy to show that the most unstable mode for the homogeneous pattern moves to lower wavevector. Investigation this possibility in detail must, however, await future studies. A final possibility is that the less differentiated cells continue to divide after the notch-dependent patterning process is completed.

## 8. Summary

In conclusion, we have studied the problem of ordered pattern formation for the realistic notch–delta system. Our main findings are as follows:

- Showing that the quasi-realistic notch–delta biological model leads to an explicit nine dimensional ODE system for ordered patterns
- Demonstrating that the exact reduction leads to an interesting co-dimension two bifurcation, which shows how the tradeoffs between hexagonal and anti-hexagonal patterns are affected by the symmetry (or lack thereof) of the ODE system. The breakdown of symmetry between the unfolding of hexagon and anti-hexagon solutions is suggested to have important biological consequences.
- The exact reduction also allows us to find analytic treatments showing the existence and stability of heretofore unrecognized solutions with correlated (instead of anti-correlated) notch versus delta patterns.
- Demonstrating that the problem of defects can in principle be solved by spatiotemporally modulating the parameters governing the transition to the patterned state.

We have argued that the presence of a pitchfork bifurcation value  $\lambda_N^{\text{PF}}$  close to the physical relevant parameter range organizes the existence and stability of high-delta centered hexagon pattern as well as the high-notch centered anti-hexagon pattern and guarantees that the former is the generic stable structure. Thus, models built on our current understanding of molecular mechanisms do help explain this recurring feature of tissue development. The importance of this is highlighted by the fact that outside the physical range of parameters, alternative correlations between notch and delta are possible. Furthermore, we have seen that creating a perfect pattern is a significant challenge in the vast majority of parameter space where the transition from the uniform state to the patterned state is second order. As already mentioned, we demonstrated that coupling a parameter to an initiation wave could provide a way to meet this challenge.

We have focused our study on the baseline patterning process enabled by the notch–delta system operating alone. In any given biological realization, there is undoubtedly coupling between this pathway and others. There are also different versions of the notch receptor and different notch ligands, used to differing effect in. These disparate settings and creating a more complex but probably more versatile system than the one we have stud-

ied here; one can of course dive into one very specific example and construct a much more complete model. We have adopted a complementary approach, analyzing in detail what occurs in the simplest case and thereby identifying the aspects of these systems that follow directly from physics and identifying those that require additional evolutionary innovation.

## Acknowledgments

ET and DAK acknowledge the support of the United States-Israel Binational Science Foundation, Grant No. 2015619. HL acknowledges the support of the NSF Grant No. PHY-1605817 and PHY-2019745. ET acknowledges useful conversations with David Sprin-  
zak.

## Data availability statement

All data that support the findings of this study are included within the article (and any supplementary files).

## Appendix A. Uniform state reduction to a single equation

When discussing uniform steady-states, it is convenient to reduce the set of three equations to a single nonlinear equation. For simplicity, we will specialize the following discussion to the case of the Hill coefficients  $n_{\pm}$  equal to 2. We first introduce the notation

$$\begin{aligned}\tilde{\lambda}_N &= \lambda_N \left( 1 + k_H \frac{I_0^2}{1 + I_0^2} \right); \\ \tilde{\lambda}_D &= \frac{\lambda_D}{1 + I_0^2}.\end{aligned}\quad (\text{A1})$$

In terms of these, we have

$$\begin{aligned}N_0 &= \frac{\tilde{\lambda}_N}{\gamma + k_0 D_0}, \\ D_0 &= \frac{\tilde{\lambda}_D}{\gamma + k_0 N_0}, \\ I_0 &= \frac{k_t \lambda_I}{\gamma_I} N_0 D_0,\end{aligned}\quad (\text{A2})$$

where we have also introduced

$$k_0 \equiv k_c + k_t. \quad (\text{A3})$$

Solving for  $N_0$  and  $D_0$  yields

$$N_0 = \frac{-k_0(\tilde{\lambda}_D - \tilde{\lambda}_N) - \gamma^2 + \sqrt{[k_0(\tilde{\lambda}_D + \tilde{\lambda}_N) + \gamma^2]^2 - 4k_0^2\tilde{\lambda}_D\tilde{\lambda}_N}}{2k_0\gamma},$$

$$D_0 = \frac{k_0(\tilde{\lambda}_D - \tilde{\lambda}_N) - \gamma^2 + \sqrt{[k_0(\tilde{\lambda}_D + \tilde{\lambda}_N) + \gamma^2]^2 - 4k_0^2\tilde{\lambda}_D\tilde{\lambda}_N}}{2k_0\gamma}, \quad (A4)$$

so that  $I_0$  satisfies

$$I_0 = \frac{k_t\lambda_I}{\gamma_I} \frac{-k_0(\tilde{\lambda}_D + \tilde{\lambda}_N) - \gamma^2 - \sqrt{[k_0(\tilde{\lambda}_D + \tilde{\lambda}_N) + \gamma^2]^2 - 4k_0^2\tilde{\lambda}_D\tilde{\lambda}_N}}{2k_0^2} \equiv \mathcal{R}(I_0). \quad (A5)$$

We next consider the stability condition for a hexagonal perturbation, which in line with the Negrete–Oates model has the form  $N_A = N_0 + \delta_N$ ,  $N_{B,C} = N_0 - \frac{1}{2}\delta_1$ ,  $D_A = D_0 + \delta_D$ ,  $D_{B,C} = D_0 - \frac{1}{2}\delta_D$ ,  $I_A = I_0 + \delta_I$ ,  $I_{B,C} = I_0 - \frac{1}{2}\delta_I$ . The stability matrix  $\mathcal{M}_U$ , is then

$$\mathcal{M}_U = \begin{pmatrix} -k_0D_0 - \gamma & (-k_c + k_t/2)N_0 & \frac{d\tilde{\lambda}_N}{dI_0} \\ (-k_c + k_t/2)D_0 & -k_0N_0 - \gamma & \frac{d\tilde{\lambda}_D}{dI_0} \\ k_t\lambda_I D_0 & -(k_t/2)\lambda_I N_0 & -\gamma_I \end{pmatrix}. \quad (A6)$$

The instability sets in when  $\text{Det } \mathcal{M}_U = 0$ , i.e., when

$$\begin{aligned} k_t\lambda_I D_0 [4\gamma + 3(k_0 + k_c)N_0] \frac{d\tilde{\lambda}_N}{dI_0} \\ = 4\gamma_I \gamma [\gamma + k_0(D_0 + N_0)] \\ + 3\gamma_I N_0 D_0 k_t (k_0 + 3k_c) \\ + 2 \frac{d\tilde{\lambda}_D}{dI_0} k_t \lambda_I N_0 (\gamma + 3k_c D_0). \end{aligned} \quad (A7)$$

To derive the condition for the bifurcation point to be a pitchfork, we consider a general nonlinear system of steady-state equations,  $f_i(x_j, \mu) = 0$ , where

the functions  $f_i$  depend on the variables  $x_j$  and the bifurcation parameter  $\mu$ . The steady-state at the bifurcation point,  $\mu_0$  is denoted  $x_{j,0}$ . At a slightly shifted value of  $\mu = \mu_0 + \Delta\mu$ , the solution is given by  $x_j = x_{j,0} + \epsilon x_{j,1}$ . Expanding the steady-state equation to first order in  $\mu$  and third order in  $\epsilon$  yields

$$\begin{aligned} 0 = \epsilon \frac{\partial f_i}{\partial x_j} x_{j,1} + \frac{\epsilon^2}{2} \frac{\partial^2 f_i}{\partial x_j \partial x_k} x_{j,1} x_{k,1} + \Delta\mu \frac{\partial f_i}{\partial \mu} \\ + \frac{\epsilon^3}{6} \frac{\partial^3 f_i}{\partial x_j \partial x_k \partial x_l} x_{j,1} x_{k,1} x_{l,1} + \epsilon \Delta\mu \frac{\partial^2 f_i}{\partial x_j \partial \mu} x_{j,1}, \end{aligned} \quad (A8)$$

where repeated indices are summed over and all derivatives are evaluated at the unperturbed solution. At the critical point,  $x_{i,1}$  is given by the right zero-mode eigenvector of the linear stability operator  $\frac{\partial f_i}{\partial x_j}$ ,  $x_{j,1} = x_j^R$ . At a pitchfork bifurcation, the second derivative terms have no projection on the zero-mode, so that

$$\frac{\partial^2 f_i}{\partial x_j \partial x_k} x_i^L x_j^R x_k^R = 0. \quad (A9)$$

The right and left eigenvectors are given by

$$x^R = \begin{pmatrix} 4\gamma_I(\gamma + k_0N_0) + 2k_t\lambda_I N_0 \frac{d\tilde{\lambda}_D}{dI_0} \\ -4\gamma_I \left(k_c - \frac{k_t}{2}\right) D_0 + 4k_t\lambda_I D_0 \frac{d\tilde{\lambda}_D}{dI_0} \\ k_t\lambda_I D_0 \left(4\gamma + 6\left(k_c + \frac{k_t}{2}\right) N_0\right) \end{pmatrix}; \quad x^L = \begin{pmatrix} k_t\lambda_I D_0 \left(4\gamma + 6\left(k_c + \frac{k_t}{2}\right) N_0\right) \\ -2k_t\lambda_I N_0 (\gamma + 3k_c D_0) \\ 4\gamma^2 + 4k_0\gamma(D_0 + N_0) + 3k_t(k_0 + 3k_c)D_0 N_0 \end{pmatrix}. \quad (A10)$$

Substituting this, the condition for a pitchfork bifurcation reads

$$0 = \frac{d^2\tilde{\lambda}_N}{dI_0^2} k_t^3 \lambda_I^3 D_0^3 [4\gamma + 3(k_0 + k_c)N_0]^3 - 2 \frac{d^2\tilde{\lambda}_D}{dI_0^2} k_t^3 \lambda_I^3 D_0^2 N_0 (\gamma + 3k_c D_0) [4\gamma + 3(k_0 + k_c)N_0]^2 \\ - 8k_t \lambda_I D_0 (\gamma + 3k_c D_0) (2\gamma + 3k_t N_0) \left[ 2k_t \lambda_I \frac{d\tilde{\lambda}_D}{dI_0} - \gamma_I (2k_c - k_t) \right] \left[ k_t \lambda_I N_0 \frac{d\tilde{\lambda}_D}{dI_0} + 2\gamma_I (\gamma + k_0 N_0) \right]. \quad (\text{A11})$$

For completeness, we note that the condition for a saddle-node bifurcation is in general

$$\frac{\partial^3 f_i}{\partial x_j \partial x_k \partial x_l} x_i^L x_j^R x_k^R x_l^R \frac{\partial f_m}{\partial \mu} x_m^L \\ = 3 \frac{\partial^2 f_i}{\partial x_j \partial x_k} x_i^L x_j^R x_k^R \frac{\partial^2 f_m}{\partial x_j \partial \mu} x_m^L x_n^R. \quad (\text{A12})$$

Using the expressions for the eigenvectors above, one can use this to derive a fairly lengthy expression for the saddle-node condition.

## Appendix B. The large $\lambda_D$ limit and the region of hexagonal instability

We showed in the main text the region of hexagonal instability in the  $k_c, \lambda_D$  plane for various  $\lambda_N$ . One striking feature of this diagram is that the phase boundaries become vertical at two critical values of  $k_c$ , so that  $\lambda_D^c(k_c)$  diverges at these values. We can derive this analytically by solve the steady-state equations in the large  $\lambda_D$  limit.

In this limit,  $D_0 \ll 1$  and  $N_0 \ll 1$ , we have

$$N_0 D_0 = \frac{\tilde{\lambda}_N}{k_0} = \frac{\gamma_I I_0}{k_t \lambda_I} \quad (\text{B1})$$

finite, which provides a closed equation for  $I_0$ . Then, the stability condition equation (A7) reduces to

$$\frac{d \ln \tilde{\lambda}_N}{d \ln I_0} = 1 + \frac{3k_c}{2k_0} \frac{d \ln \tilde{\lambda}_D}{d \ln I_0}. \quad (\text{B2})$$

Doing the algebra, we find that the critical  $I_0$  satisfies the equation

$$3\gamma_I (1 + I_0^2) I_0^3 = \lambda_I \lambda_N [I_0^2 (1 + 2I_0^2) (1 + k_H) - 1]. \quad (\text{B3})$$

This equation typically has two positive roots for  $I_0$ , which when substituted back into equation (A5) yields the critical value of  $k_0/k_c = 1 + k_t/k_c$ . We also see that the critical  $k_t/k_c$  only depends on the lumped

parameter  $\xi \equiv \lambda_I \lambda_N / \gamma_I$  and  $k_H$ . For large  $\xi$ , things simplify further and we find the solutions

$$I_0 \approx \frac{2}{3} \xi (1 + k_H); \quad I_0 \approx \frac{1}{2} \left[ \sqrt{\frac{k_H + 9}{k_H + 1}} - 1 \right]^{1/2}, \quad (\text{B4})$$

corresponding to

$$\frac{k_t}{k_c} \approx 2; \quad \frac{k_t}{k_c} \approx \frac{1 + k_H}{\xi} \left[ \sqrt{\frac{k_H + 9}{k_H + 1}} - 1 \right]^{1/2}. \quad (\text{B5})$$

In figure B1, we plot the two solutions for  $k_t/k_c$  as a function of  $\lambda_N$  for the standard parameters  $k_H = 1$ ,  $\lambda_I = 1$ ,  $\gamma_I = 1/2$ . We see that for  $\xi \gtrsim 1$ , there are two critical values of  $k_t/k_c$ , one near 0 and the other near 2, between which the uniform solution is unstable to a hexagonal pattern. This behavior is manifest in the numerical unstable region plotted in figure 5 in the main text.

## Appendix C. The large $\lambda_N$ limit and the region of hexagonal instability

Similarly, we can compute the region of hexagonal instability for large  $\lambda_N$ . Here,  $N_0$  is large and  $D_0$  is small, with the product being of order 1:

$$N_0 D_0 \approx \frac{\tilde{\lambda}_D}{k_0} = \frac{I_0 \gamma_I}{k_t \lambda_I}. \quad (\text{C1})$$

Then, the stability criterion reads

$$\frac{d \ln \tilde{\lambda}_D}{d \ln I_0} = \frac{3(k_c + k_0)}{2k_0} \frac{d \ln \tilde{\lambda}_N}{d \ln I_0} - 2 \quad (\text{C2})$$

which reduces to

$$1 = \frac{I_0^2}{1 + I_0^2} + \frac{3I_0^2 k_H (k_c + k_0)}{2k_0 (1 + I_0^2) (1 + I_0^2 (1 + k_H))}. \quad (\text{C3})$$

Eliminating  $k_t/k_c$  yields an equation for  $I_0$  in terms of  $k_H$  and the lumped parameter  $\zeta = \lambda_D \lambda_I / \gamma_I$

$$3I_0^3 k_H = 2 [1 + I_0^2 (1 + 2k_H)] \zeta \quad (\text{C4})$$

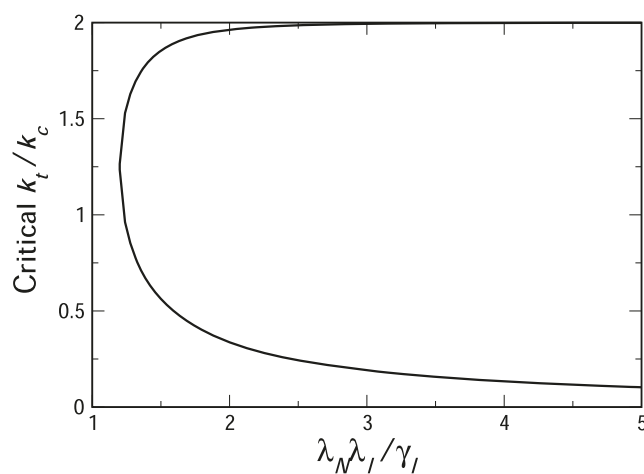


**Figure B1.** The two critical values of  $k_t/k_c$  as a function of  $\xi = \lambda_N\lambda_I/\gamma_I$ , for  $k_H = 1$  in the large  $\lambda_D$  limit. We see that in line with our analytic calculation, for large  $\xi$ , the critical  $k_t/k_c$  either approaches 2 or 0.

yielding for  $I_0$ ,

$$I_0^2 = \frac{2k_0}{k_t(4k_H - 2) + k_t(k_H - 2)}. \quad (\text{C5})$$

Substituting this into equation (C1) and solving for  $\zeta$  yields

$$\zeta = \sqrt{2}k_H \frac{k_t + 4k_c}{k_t} \left( \frac{k_t + k_c}{k_c(4k_H - 2) + k_t(k_H - 2)} \right)^{3/2}. \quad (\text{C6})$$

This solution, which specifies the critical value of  $\zeta$  (or  $\lambda_D$  for given  $\lambda_I$  and  $\gamma_I$ ) is physical only if  $k_c/k_t > (2 - k_H)/2(2k_H - 1)$ . This relation, plotted in figure 5 for  $k_H = 2/3$  and  $k_H = 4/3$  shows that  $\zeta$  decreases from infinity as  $k_t$  increases from 0, reaches a minimum and then increases, diverging as  $k_t/k_c$  approaches  $(2 - k_H)/2(2k_H - 1)$ . The graph is similar for all  $1/2 \leq k_H < 2$ . For  $k_H < 1/2$  there is no critical  $\lambda_D$  for large  $\lambda_N$ , whereas for  $k_H > 2$ , there is a critical  $\lambda_D$  for all  $k_t/k_c$ .

It should be noted that our results for large  $\lambda_D$  indicated that the point of divergence of  $\lambda_D$  is close to  $k_t = 2k_c$  for large  $\lambda_N$ . However, our current large  $\lambda_N$  calculation indicates that  $\lambda_D$  diverges at  $k_t = [(2 - k_H)/2(2k_H - 1)]k_c$ . This indicates that the large  $\lambda_D$  and large  $\lambda_N$  limits do not commute. This is reflected especially in the right panel of figure 5 in the main text, where for  $k_H = 4/3$ , we see that for large finite  $\lambda_N$ ,  $\lambda_D$  appears to be diverging at the location predicted by the large  $\lambda_N$  calculation, but once  $\lambda_D$  is sufficiently large, it turns back at the curve eventually approaches the  $k_t = 2k_c$  line.

## Appendix D. Multiple uniform states

We have found through numerical experiments parameter regions that show the existence of multiple uniform states. Here we want to clarify where in parameter space such solutions exist. We start by

again assuming large  $\lambda_D$ . We get, following the same scaling as above,

$$I_0 = \mathcal{R}(I_0) \equiv \frac{k_t\lambda_N \left( 1 + k_H \frac{I_0^2}{1+I_0^2} \right)}{\gamma_I k_0}. \quad (\text{D1})$$

There are either 1 or 3 solutions of this nonlinear equation. The bifurcation point is where these three solutions collapse to 1. At this point,

$$0 = \mathcal{R}' - 1 = \mathcal{R}''. \quad (\text{D2})$$

Denoting  $Q \equiv \frac{k_t\lambda_N}{\gamma_I k_0}$ , this reads

$$1 = 2Qk_H \frac{I_0}{(1 + I_0^2)^2},$$

$$0 = 2Qk_H \frac{1 - 3I_0^2}{1 + I_0^2}. \quad (\text{D3})$$

Thus, from the second of these, at the bifurcation,  $I_0^* = \sqrt{3}/3$ . The first then implies  $k_H^* = \frac{8\sqrt{3}}{9Q^*}$ . Plugging these into equation (D1) gives

$$Q^* = \frac{\sqrt{3}}{9}, \quad (\text{D4})$$

so that

$$k_H^* = 8. \quad (\text{D5})$$

To see how things look in the vicinity of the bifurcation point, we write  $Q = Q^* + \delta_Q$ ,  $k_H = k_H^* + \delta_k$ ,  $I_0 = I_0^* + \delta_I$ . Expanding to third order in  $\delta_I$ , equation (D1) translates to

$$0 = 1/36(\sqrt{3}\delta_k + 108\delta_Q + 9\delta_k\delta_Q)$$

$$+ 1/8(\delta_k + 24\sqrt{3}\delta_Q + 3\sqrt{3}\delta_k\delta_Q)\delta_I$$

$$- 3/32(8 + \delta_k + 24\sqrt{3}\delta_Q + 3\sqrt{3}\delta_k\delta_Q)\delta_I^3. \quad (\text{D6})$$

In the last term, we can drop all the  $\delta_k$ ,  $\delta_Q$  pieces as being higher order. Then, for the second term to be

the same order as the third, we have to have that  $\delta_k$ ,  $\delta_Q$  are both of order  $\delta_I^2$ , and we can drop the last piece of the second term. To make the first term also of the same order, its leading contribution must vanish, so that  $\delta_Q = -\sqrt{3}/108\delta_k + \alpha\delta_k^{3/2}$ . Then, the equation reduces to

$$0 = \frac{1}{36} \left( 108\alpha\delta_k^{3/2} \right) + \frac{1}{8} \left( \frac{2}{3}\delta_k \right) \delta_I - \frac{3}{4}\delta_I^3. \quad (\text{D7})$$

To have three solutions, we must have  $\delta_k > 0$ , so that the derivative of this equation has two solutions. Then, there are solutions in a band around  $\delta_Q = -\sqrt{3}/108\delta_k$ , which is negative. Performing the numerical solution for large but finite  $\lambda_D$  yields the same conclusions, with  $k_H^*$  rising as  $\lambda_D$  falls. As we take

$\lambda_D$  smaller and smaller,  $k_H^*$  continues to rise, and eventually diverges at a finite value of  $\lambda_D$ . This is shown in figure D1. We will calculate this value momentarily, but the implication is clear: there are only multiple uniform solutions for  $k_H > 8$ , which is much larger than physical. This is all the more so since  $\lambda_D$  is finite, and the multiple uniform solution lower bound on  $k_H$  is thus in fact much higher.

Our last task is to determine the minimal value,  $\lambda_D^*$  below which multiple uniform solutions are impossible. The numerics show that as  $\lambda_D$  approaches its critical value,  $I_0^*$  approaches 0 as  $k_H^*$  diverges, with  $k_H^*(I_0^*)^2$  remaining finite. In this limit, denoting  $x = k_H I_0^2$ , we have

---


$$R_0(I_0) = \frac{Q}{2} \left[ \frac{\lambda_D}{\lambda_N} + \frac{\gamma_D \gamma_N}{k_0 \lambda_N} + 1 + x - \sqrt{\left( \frac{\lambda_D}{\lambda_N} + \frac{\gamma_D \gamma_N}{k_0 \lambda_N} + 1 + x \right)^2 - 4 \frac{\lambda_D(1+x)}{k_0}} \right]. \quad (\text{D8})$$


---

We introduce the notation  $\sigma = \frac{\gamma_D \gamma_N}{k_0 \lambda_N}$ ,  $A = \frac{\lambda_D}{\lambda_N} + \sigma + 1$ ,  $B = 4\frac{\lambda_D}{\lambda_N}$  and rewrite

$$R_0(I_0) = \frac{Q}{2} \left( A + x - \sqrt{(A+x)^2 - B(1+x)} \right). \quad (\text{D9})$$

At the bifurcation point, we have  $R_0(I_0) = 0$ ,  $R'_0(I_0) = 0$ , and  $R''_0(I_0) = 0$ , where the derivatives are not w.r.t.  $x$ . Proceeding, we find the solution

---


$$x^* = A/3; \quad B^* = \frac{4A^2}{3}(1 - A/9); \quad Q^* = \frac{3\sqrt{3}}{\sqrt{A}(9-A)}. \quad (\text{D10})$$


---

Given  $B^*$ , since

$$1 + \frac{\gamma_D \gamma_N}{k_0 \lambda_N} = A - B/4 \quad (\text{D11})$$

we have that

$$A = 3 \left( 1 + [\sigma]^{1/3} \right). \quad (\text{D12})$$

This corresponds to a critical value of  $\lambda_D/\lambda_N$  at which  $k_H^*$  diverges of

$$\frac{\lambda_D}{\lambda_N} = \left[ 1 + \sigma^{1/3} \right]^2 \cdot \left[ 2 - \sigma^{1/3} \right]. \quad (\text{D13})$$

Examining this, we see that there is a maximum of  $\lambda_D/\lambda_N$  for  $\sigma = 1$ . Also, there is a change of behavior for  $\sigma > 8$ . Above this value,  $k_H^*$  remains finite down to  $\lambda_D = 0$ , and  $\lambda_D = 0$  it is a decreasing function of  $\sigma$ , approaching  $10 + 4\sqrt{6}$  from above as  $\sigma \rightarrow \infty$ . In general, as  $\sigma$  gets large,  $k_H^*$  is a monotonically decreasing function of  $\lambda_D/(\lambda_N\sigma)$ , going between  $10 + 4\sqrt{6}$  at  $\lambda_D/\sigma \rightarrow 0$  and 8 as  $\lambda_D/\sigma \rightarrow \infty$ :

---


$$k_H^* = \frac{320 + 464\frac{\lambda_D}{\lambda_N\sigma} + 160\left(\frac{\lambda_D}{\lambda_N\sigma}\right)^2 + 7\left(\frac{\lambda_D}{\lambda_N\sigma}\right)^3 + \sqrt{96 + 96\frac{\lambda_D}{\lambda_N\sigma} + 9\left(\frac{\lambda_D}{\lambda_N\sigma}\right)^2} \left( 32 + 32\frac{\lambda_D}{\lambda_N\sigma} + 3\left(\frac{\lambda_D}{\lambda_N\sigma}\right)^2 \right)}{2 \left( 1 + \frac{\lambda_D}{\lambda_N\sigma} \right) \left( 16 + 16\frac{\lambda_D}{\lambda_N\sigma} + \left(\frac{\lambda_D}{\lambda_N\sigma}\right)^2 \right)}. \quad (\text{D14})$$


---

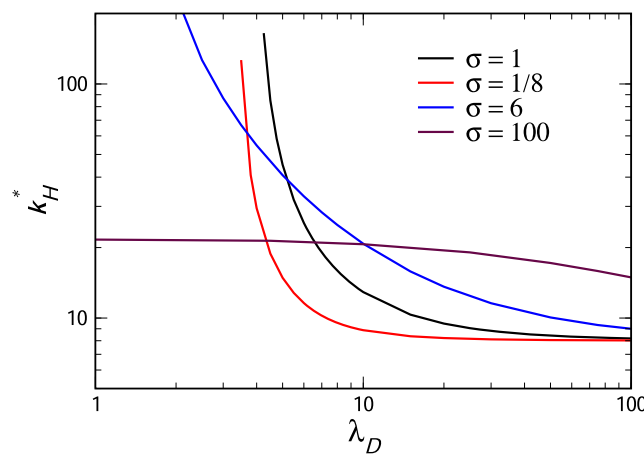


**Figure D1.** The critical value  $k_H^*$  above which multiple uniform solutions are possible (for some range of  $Q$ ).  $\sigma \equiv \frac{\gamma_D \gamma_N}{k_0 \lambda_N} = 1, 1/8$ , and 6, and 100.

## Appendix E. Hexagonal symmetry steady-state equation

As discussed in the main text, one can reduce the full system of equations to a coupled ODE system. If we specialize to the case of steady-state patterns with hexagonal symmetry, so that the  $B$  and  $C$  sublattices are equivalent, we obtain the six-dimensional system

$$\begin{aligned}
 0 &= \lambda_N H_+(I_A) - N_A (k_c D_A + k_t D_B) - \gamma N_A \\
 0 &= \lambda_D H_-(I_A) - D_A (k_c N_A + k_t N_B) - \gamma D_A \\
 0 &= k_t N_A D_B - \gamma_I I_A \\
 0 &= \lambda_N H_+(I_B) - N_B \left( k_c D_B + \frac{k_t}{2} (D_A + D_B) \right) \\
 &\quad - \gamma N_B \\
 0 &= \lambda_D H_-(I_B) - D_B \left( k_c N_A + \frac{k_t}{2} (N_B + N_A) \right) \\
 &\quad - \gamma D_B \\
 0 &= \frac{k_t}{2} \lambda_I N_B (D_A + D_B) - \gamma_I I_A. \tag{E1}
 \end{aligned}$$

## Appendix F. Hi–Hi solutions

In the main text, we discussed the fact that the model as presented can support anomalous solutions in which the levels of notch and delta are positively correlated in the different sub-lattice sites instead of

being anti-correlated. To study this in more detail, we look analytically at the large  $\lambda_D$  limit and look for the critical curve along which notch on the  $A$  and  $B$  sublattice sites are equal. This curve should demarcate the boundary between regular hexagonal solutions and what we are calling Hi–Hi solutions. Studying the numerics (data not shown), we see that  $D_A$  and  $D_B$  are large, of order  $\lambda_D$  and  $N_A = N_B \equiv N$  is small, of order  $1/\lambda_D$ . Writing  $N_A = N_B = N_0/\lambda_D$ ,  $D_A = \lambda_D D_{A0}$ ,  $D_B = \lambda_D D_{B0}$  and specializing to the case of Hill coefficient 2 in the transcriptional/regulation terms, we have to solve the system

$$\begin{aligned}
 \lambda_N \left( 1 + \frac{k_H I_A^2}{1 + I_A^2} \right) &= k_T N_0 D_{B0} + k_c N_0 D_{A0}, \\
 \lambda_N \left( 1 + \frac{k_H I_B^2}{1 + I_B^2} \right) &= \frac{1}{2} k_T N_0 (D_{A0} + D_{B0}) \\
 &\quad + k_c N_0 D_{B0}, \\
 \frac{1}{1 + I_A^2} &= \gamma D_{A0}, \\
 \frac{1}{1 + I_B^2} &= \gamma D_{B0}, \\
 k_t \lambda_I N_0 D_{B0} &= \gamma_I I_A, \\
 \frac{1}{2} k_t \lambda_I N_0 (D_{A0} + D_{B0}) &= \gamma_I I_B. \tag{F1}
 \end{aligned}$$

Here we have chosen units such that  $s_0 = 1$ . This system admits two exact solutions, in terms of  $\eta \equiv \frac{\lambda_N \lambda_I (1 + k_H)}{\gamma_I}$ :

$$\begin{aligned}
 I_A &= \frac{\eta \pm \sqrt{\eta^2 - 12}}{3} \\
 I_B &= \frac{5\eta \mp \sqrt{\eta^2 - 12}}{6}
 \end{aligned}$$

$$\begin{aligned}
D_{A0} &= \frac{1}{\gamma(1 + I_A^2)} \\
D_{B0} &= \frac{1}{\gamma(1 + I_B^2)} \\
N_0 &= \frac{\gamma\gamma_I I_A(1 + I_B^2)}{k_t} \\
k_c &= k_t \frac{\eta^2(17 - k_H) \pm 3k_H\eta\sqrt{\eta^2 - 12} \pm 2k_H\eta^3\sqrt{\eta^2 - 12} + 4(1 + k_H) + 2\eta^4(2 + k_H)}{2(4 + \eta^2)(1 + 4\eta^2)(1 + k_H)}. \quad (F2)
\end{aligned}$$

The two solutions merge at  $\eta = \sqrt{12}$  and do not exist for  $\eta < \sqrt{12}$ . One key result is that the critical  $k_c$  is proportional to  $k_t$ . For large  $\eta$ , which is typical for our parameters where  $\gamma = 0.1$ , things simplify tremendously and we have for the ‘-’ branch:

$$\begin{aligned}
I_A &= \frac{2}{\eta} \ll 1, \\
I_B &= \eta \gg 1, \\
D_{A0} &= \frac{1}{\gamma}, \\
D_{B0} &= \frac{1}{\gamma\eta^2} \ll 1, \\
N_0 &= \frac{2\gamma\gamma_I\eta}{\lambda_I k_t} \gg 1, \\
k_c &= \frac{k_t}{2(1 + k_H)}. \quad (F3)
\end{aligned}$$

In fact, for  $\eta = \sqrt{12}$  which is its lower limit, we get  $k_c/k_t = (14 + 5k_H)/28/(1 + k_H)$ , which is only slightly higher than the infinite  $\eta$  result.

Going off this border line numerically, we find that the solution to the left of the line is a Hi–Hi solution, whereas to the right is a regular hexagon. The branch starting from the ‘-’ border is stable whereas starting from the ‘+’ border is unstable. Thus, the two solutions are completely distinct, even in the region to the right of both borders. The region of stable Hi–Hi solutions extends all the way down to  $k_c = 0$ . The relevant phase diagram is shown in figure 9. We show the line above which stable Hi–Hi solutions exist, and below which stable Hi–Lo hexagons exist, both of which coexist with a stable uniform solution. We also show the saddle-node bifurcation line, below which only the uniform solution is stable.

## Appendix G. Disordered lattice

Our baseline model takes the form

$$\begin{aligned}
\dot{N}_x &= \lambda_N H_+(I_x) - N_x (k_c D_x + k_t D_x^{\text{ext}}) - \gamma N_x \\
\dot{D}_x &= \lambda_D H_-(I_x) - D_x (k_c N_x + k_t N_x^{\text{ext}}) - \gamma D_x \\
\dot{I}_x &= k_t \lambda_I N_x D_x^{\text{ext}} - \gamma_I I_x. \quad (G1)
\end{aligned}$$

Here, positions  $x$  refer to locations on an hexagonal lattice and the superscript ‘ext’ refers the average over the six nearest neighbor sites of  $x$ .

We now want to allow for the possibility of a disordered lattice. Let us continue to define all the variables,  $N_x$ ,  $D_x$  and  $I_x$  as the total number of these molecules for a cell with center point  $x$ . Then, the form of the three decay terms and the  $N$  and  $D$  production terms do not need to be changed. For the *cis* and *trans* interaction interaction term, let us define the ‘intensive’ parameters  $\hat{k}_c$  and  $\hat{k}_t$ . Starting with the *cis* term, and assuming uniform concentrations along the membrane, we have for cell  $x$

$$\sum_i \ell_{x,i} \hat{k}_c \left( \frac{N_x}{L_x} \right) \left( \frac{D_x}{L_x} \right),$$

where  $\ell_{x,i}$  is the length of the  $i$ th edge of cell  $x$  and  $L_x = \sum_i \ell_{x,i}$  is the perimeter of cell  $x$ . Since nothing depends on  $i$ , we immediately obtain

$$\frac{\hat{k}_c}{L_x} N_x D_x.$$

We then define  $\hat{k}_c \equiv \langle L_x \rangle k_c$  ( $\langle \cdot \rangle$  means average over the lattice) to ensure that the regular lattice limit agrees with the original model. The final expression is then

$$\frac{k_c \langle L_x \rangle}{L_x} N_x D_x.$$

The *trans* term is treated the same way. The basic expression is

$$\sum_i \ell_{x,i} \hat{k}_t \left( \frac{N_x}{L_x} \right) \left( \frac{D_{x,i}}{L_{x,i}} \right),$$

where the notation  $x; i$  refers to the neighboring cell that shares edge  $i$  with the cell at  $x$ . Using the same reparameterization  $\hat{k}_t \equiv \langle L_x \rangle k_t$ , we obtain

$$\sum_i \ell_{x,i} k_t \langle L_x \rangle \left( \frac{N_x}{L_x} \right) \left( \frac{D_{x,i}}{L_{x,i}} \right).$$

Next, we discuss how we generate disordered lattices. Specifically, we use the idea of a CRN that was originally introduced to model semiconductors [34]. We introduce a set of  $n$  ‘atoms’ each of which is connected by bonds to three neighbors with which it

interacts. The interaction energy is given by

$$E_{\text{tot}} = \sum_{j=1}^n \sum_{i=1}^3 \left[ \frac{1}{4} k_r (|\vec{r}_{ji}| - a)^2 + \frac{1}{2} k_\theta \left( \cos \theta_{ji} - \cos \frac{2\pi}{3} \right)^2 \right]. \quad (\text{G2})$$

We start from a perfect honeycomb lattice. We pick two nearby bonds, and attempt to reattach them so that the first bond now connects on of the atoms on its ends with an atom on the end of the second bonds, and vice versa, following the Monte Carlo scheme originally devised in reference [34]. We accept the change with probability unity if it lowers the energy and with probability  $\exp(-\Delta E/T)$  if it raises the energy. The final result is a perturbed lattice, with a number of the perfect-lattice hexagons replaced by pentagons, heptagons and the occasional quadrilateral and octagon.

In our simulations, we chose  $a = 4$ ,  $k_r = k_\theta = 1$ , and attempted 2000 bond exchanges. The more ordered lattice, used in figure 11(a), used  $T = 0.3$ , resulted in roughly 10% nonhexagonal cells and the more disordered lattice in figure 11(b) used  $T = 0.6$ , yielding roughly 25% nonhexagonal cells. In the third simulation panel we used  $T = 1.1$ . In addition, we generated a system slightly larger than that presented in the figure, and then eliminated the outermost row of cells on each side, in order to obtain a more accurate measure of the fraction of hexagons. For the less-disordered systems, this proved unnecessary. The speed of the wave was chosen as  $v = 0.01$  in all cases, in units where  $\langle L \rangle = 24$ .

## ORCID iDs

David A Kessler  <https://orcid.org/0000-0002-5279-1655>

Herbert Levine  <https://orcid.org/0000-0002-8819-9055>

## References

- [1] Andersson E R, Sandberg R and Lendahl U 2011 Notch signaling: simplicity in design, versatility in function *Development* **138** 3593
- [2] Gazave E, Lapébie P, Richards G S, Brunet F, Ereskovsky A V, Degnan B M, Borchiellini C, Vervoort M and Renard E 2009 Origin and evolution of the notch signalling pathway: an overview from eukaryotic genomes *BMC Evol. Biol.* **9** 249
- [3] Artavanis-Tsakonas S, Matsuno K and Fortini M 1995 Notch signaling *Science* **268** 225
- [4] Neves J, Abelló G, Petrovic J and Giraldez F 2013 Patterning and cell fate in the inner ear: a case for notch in the chicken embryo *Dev., Growth Differ.* **55** 96
- [5] Chen K Y *et al* 2017 A notch positive feedback in the intestinal stem cell niche is essential for stem cell self-renewal *Mol. Syst. Biol.* **13** 927
- [6] Kaylan K B *et al* 2018 *eLife* **7** e38536
- [7] Bray S and Bernard F 2010 Notch targets and their regulation *Curr. Top. Dev. Biol.* **92** 253
- [8] Shaya O and Sprinzak D 2011 From notch signaling to fine-grained patterning: modeling meets experiments *Curr. Opin. Genet. Dev.* **21** 732
- [9] Fanto M and Mlodzik M 1999 Asymmetric notch activation specifies photoreceptors R3 and R4 and planar polarity in the *Drosophila* eye *Nature* **397** 523
- [10] Boareto M, Jolly M K, Goldman A, Pietilä M, Mani S A, Sengupta S, Ben-Jacob E, Levine H and Onuchic J N 2016 Notch–jagged signalling can give rise to clusters of cells exhibiting a hybrid epithelial/mesenchymal phenotype *J. R. Soc., Interface* **13** 20151106
- [11] Zhu H, Zhou X, Redfield S, Lewin J and Miele L 2013 Elevated Jagged-1 and Notch-1 expression in high grade and metastatic prostate cancers *Am. J. Transl. Res.* **5** 368
- [12] Adam J, Myat A, Le Roux I, Eddison M, Henrique D, Ish-Horowicz D and Lewis J 1998 Cell fate choices and the expression of notch, delta and Serrate homologues in the chick inner ear: parallels with *Drosophila* sense-organ development *Development* **125** 4645
- [13] Du X, Osterfield M and Shvartsman S Y 2014 Computational analysis of three-dimensional epithelial morphogenesis using vertex models *Phys. Biol.* **11** 066007
- [14] Collier J R, Monk N A M, Maini P K and Lewis J H 1996 Pattern formation by lateral inhibition with feedback: a mathematical model of delta–notch intercellular signalling *J. Theor. Biol.* **183** 429
- [15] Sprinzak D, Lakhanpal A, LeBon L, Santat L A, Fontes M E, Anderson G A, Garcia-Ojalvo J and Elowitz M B 2010 Cis-interactions between notch and delta generate mutually exclusive signalling states *Nature* **465** 86
- [16] Formosa-Jordan P and Ibañes M 2009 Diffusible ligand and lateral inhibition dynamics for pattern formation *J. Stat. Mech.* **P03019**
- [17] Formosa-Jordan P and Ibañes M 2014 Competition in notch signalling with cis enriches cell fate decisions *PLoS One* **9** e95744
- [18] Formosa-Jordan P and Sprinzak D 2014 Modeling notch signalling: a practical tutorial *Notch Signaling* (Berlin: Springer) pp 285–310
- [19] Glass D S, Jin X and Riedel-Kruse I H 2016 Signaling delays preclude defects in lateral inhibition patterning *Phys. Rev. Lett.* **116** 128102
- [20] Negrete J Jr and Oates A C 2019 *Phys. Rev. E* **99** 042417
- [21] Sheldon B L and Milton M K 1972 Studies on the scutellar bristles of *Drosophila melanogaster*: II. Long-term selection for high bristle number in the Oregon RC strain and correlated responses in abdominal chaetae *Genetics* **71** 567
- [22] Shaya O *et al* 2017 Cell–cell contact area affects notch signalling and notch-dependent patterning *Dev. Cell* **40** 505
- [23] Corson F, Couturier L, Rouault H, Mazouni K and Schweisguth F 2017 Self-organized notch dynamics generate stereotyped sensory organ patterns in *Drosophila* *Science* **356** eaai7407
- [24] Boareto M, Jolly M K, Lu M, Onuchic J N, Clementi C and Ben-Jacob E 2015 Jagged-delta asymmetry in notch signalling can give rise to a sender/receiver hybrid phenotype *Proc. Natl Acad. Sci. USA* **112** E402
- [25] Formosa-Jordan P 2013 Pattern formation through lateral inhibition mediated by notch signalling *PhD Thesis* Universitat de Barcelona
- [26] Cross M C and Hohenberg P C 1993 Pattern formation outside of equilibrium *Rev. Mod. Phys.* **65** 851
- [27] Busse F H 1978 Non-linear properties of thermal convection *Rep. Prog. Phys.* **41** 1929
- [28] Strogatz S H 2015 *Nonlinear Dynamics and Chaos: With Applications to Physics, Biology, Chemistry, and Engineering* 2nd edn (Boca Raton, FL: CRC Press)
- [29] Barad O, Rosin D, Hornstein E and Barkai N 2010 Error minimization in lateral inhibition circuits *Sci. Signaling* **3** ra51

- [30] Barad O, Hornstein E and Barkai N 2011 Robust selection of sensory organ precursors by the notch–delta pathway *Curr. Opin. Cell Biol.* **23** 663
- [31] Formosa-Jordan P, Ibáñez M, Ares S and Fraile J M 2012 Regulation of neuronal differentiation at the neurogenic wavefront *Development* **139** 2321
- [32] Pennington M W and Lubensky D K 2010 Switch and template pattern formation in a discrete reaction–diffusion system inspired by the *Drosophila* eye *Eur. Phys. J. E* **33** 129
- [33] Lubensky D K, Pennington M W, Shraiman B I and Baker N E 2011 A dynamical model of ommatidial crystal formation *Proc. Natl Acad. Sci. USA* **108** 11145
- [34] Cohen M, Georgiou M, Stevenson N L, Miodownik M and Baum B 2010 Dynamic Filopodia transmit intermittent delta–notch signaling to drive pattern refinement during lateral inhibition *Dev. Cell* **19** 78
- [35] Lu J *et al* 2013 Endothelial cells promote the colorectal cancer stem cell phenotype through a soluble form of jagged-1 *Cancer Cell* **23** 171